中国激光

飞秒激光诱导医用金属材料表面功能微纳结构的研究进展

王翼猛[1]，管迎春[1,2,3,4*]

[1]北京航空航天大学机械工程与自动化学院，北京 100083；

[2]北京航空航天大学大型金属构件增材制造国家工程实验室，北京 100083；

[3]北京航空航天大学国际交叉科学研究院，北京 100083；

[4]北京航空航天大学宁波创新研究院，浙江 宁波 315800

摘要 随着社会发展和医疗健康事业的进步，医用金属植入物等医疗器械在临床应用中出现的细菌感染、生物相容性不佳等瓶颈亟待解决。近年来，飞秒激光以其加工精度高、适用材料广、热效应低、灵活可靠等优势，成为医用材料表面改性备受关注的新技术。本文针对体液光谱检测、植入物表面细胞行为调控、口腔抗菌这三个具体临床应用场景，简述了制备表面微纳复合结构实现生物功能的基本原理，以及多功能微纳复合结构的制备原理，梳理了飞秒激光诱导微纳结构的应用进展及研究现状，以期为相关研究人员提供线索和依据。

关键词 激光技术；飞秒激光；微纳结构；功能表面；生物相容性；光谱检测

中图分类号 R318.08 **文献标志码** A **DOI**：10.3788/CJL202249.1002601

1 引 言

由于人口老龄化以及现代生活方式的改变，数以万计的患者被骨科、口腔和面部疾病所困扰[1]。临床医疗对于高质量医疗器械及植入物的需求日益旺盛。与传统的医用无机非金属材料及医用高分子材料相比，医用金属材料具有更优异的综合力学性能和加工成型能力[2]。目前，在临床上应用的医用金属多为惰性材料，包括不锈钢、钴基合金和钛基合金等[3]。不锈钢作为一类临床应用最为广泛的材料，制备简单，但其力学性能和耐蚀性逊于钴基合金。然而，钴基合金的制作加工非常困难[4]。商用纯钛（CP-Ti）及 TC4（Ti6Al4V）等由于比强度高、耐蚀性优良等成为临床植入物材料[5-6]。但是，TC4 等材料的弹性模量高于人体骨骼，并且 Al、V 等元素对人体具有一定的毒性[7]，因此，研究人员近年来开发了诸如 Ti-Zr[8]、Ti-Nb[9]、Ti-13Nb-13Zr[10]、Ti-35Nb-5Ta-7Zr[11]、Ti-29Nb-13Ta-4.6Zr[12]、Ti-38.3Ta-22Zr-8.1Nb[13]等新型医用钛合金材料。考虑到惰性材料植入物要长期在患者体内服役或二次取出，易造成毒性离子释放带来并发症[14]，研究人员开发了镁合金、锌合金等一系列可降解植入物。镁元素是人体必需的微量元素，而镁合金植入物由于可降解且力学性能接近人体骨骼，成为一类理想的植入物选择材料[15]。镁合金作为心血管支架及骨修复材料的研究有着悠久的历史[16]。20 世纪初，Payr[17]首次尝试将镁合金应用于骨修复；Lambotte[18]在 1906 年首次将镁合金用于骨折内固定。但由于镁合金的降解速度快，且会产生大量氢气，导致炎症，因此在一段时间内被钛合金、不锈钢材料所取代。随着本世纪以来镁合金冶金技术的发展，新型可降解镁合金材料再次得到研究人员的关注。此外，金、银、铂等贵重金属及高熵合金、大块非晶合金等其他金属材料以其独特的性能，也在临床医疗中发挥着重要作用[19]。研

收稿日期：2021-11-30；**修回日期**：2022-01-25；**录用日期**：2022-01-26

基金项目：北京市自然科学基金—海淀原始创新联合基金（L202006）、宁波市“科技创新 2025”重大专项（2020Z071）

通信作者：*guanyingchun@buaa.edu.cn

发具有良好生物相容性、力学性能以及组织愈合诱导性能的生物材料具有重大意义[20]。图 1 展示了常见金属植入物的应用场景，表 1 展示了常见医用金属材料的主要应用场景及特点。

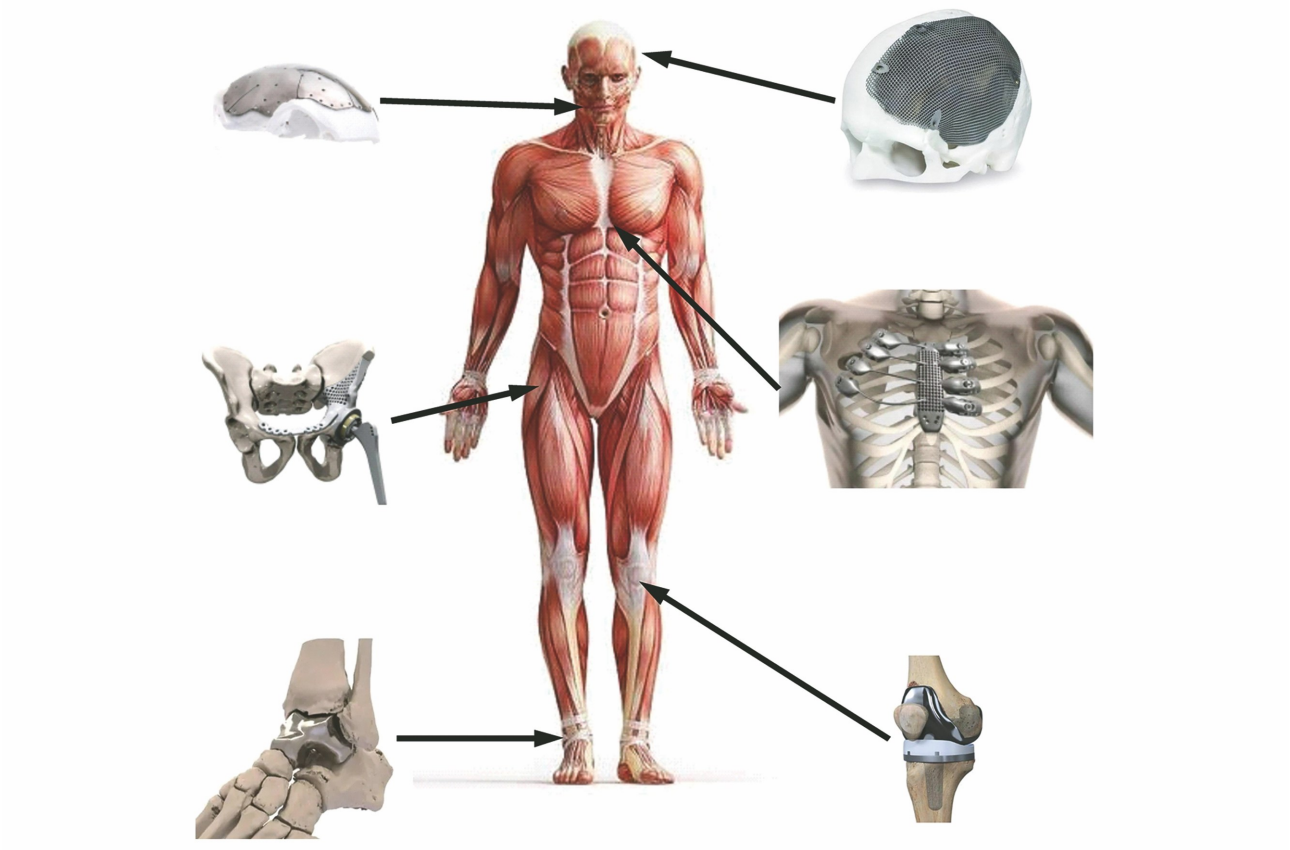

图 1 典型金属植入物的临床应用场景

Fig. 1 Typical metal implant applications

表 1 常见医用金属材料的临床应用

Table 1 Clinical application of common medical metal materials

Type of medical material		Main clinical application	Application advantage	Main limitation	Ref.
Inert	Stainless steel	Widely used in various fields such as stomatology, fracture internal fixation instruments, and artificial joints	Low cost, good processability and mechanical properties	The toxicity and corrosion resistance of alloy elements are weaker than those of cobalt base alloys	[21]
	Cobalt base alloy	Manufacturing and processing is very difficult	The mechanical properties and corrosion resistance are better than those of stainless steel	The joint replaces the trunk of the prosthesis connector	[22]
	Titanium base alloy	Surgical implants and orthopaedic instrument products	The density is similar to human bone, the new brand is non-toxic, light and has high strength and good biocompatibility	Young's modulus is higher than that of human bones and traditional alloy elements	[23]

（续表）

Type of medical material		Main clinical application	Application advantage	Main limitation	Ref.
Inert	Aluminum base alloy	High load components	Good plasticity and biocompatibility, high corrosion resistance in body fluids, high alternating fatigue strength, and no receptor fluid	Notch crack growth capability is high	[24]
	Zirconium base alloy	Replace human hard tissue	High strength, good toughness and corrosion resistance, good biocompatibility, and appropriate elastic modulus	Zirconium is often used as an additive element in titanium implants, and its alloy system design for preparation needs to be further studied	[25]
Degradable	Magnesium base alloy	Tissue and organ wound repair and functional reconstruction represented by degradable magnesium alloy vascular stent	Biocompatibility, mechanical compatibility and biodegradability are favorable for cell growth, differentiation and transportation	Degradation rate regulation	[26]
	Zinc base alloy	Bone defect implant	Zinc is a trace element needed by human body	The mechanical properties and biocompatibility still need to be adjusted by the addition of alloy elements	[27]
	Tungsten	Mechanical detachable coil embolization for intracranial aneurysms	Radiation impermeability and good biocompatibility	Degraded tungsten is enriched in blood vessels and has certain thrombogenicity	[28]
Precious metals		Dental implant material, artificial heart power supply (Pt), sterilization (Ag), clinical detection (Au and Ag)	Unique biocompatibility, good ductility, and non-toxic to human body	High cost	[29]
Other metal materials		Bone plate, screw, pacemaker, etc.	High strength, high hardness, high wear and corrosion resistance, high fatigue resistance, and suitable elastic modulus	The design of alloy system for preparation needs to be further studied	[30]

除了材料种类，医疗器械及植入物的表面状态也是治疗方案能否取得成功的重要因素[31]。表面状态会影响附近组织的细胞增殖分化[32]、骨整合[33]、免疫应答[34]、神经递质释放与运输[35]、细菌感染[36]等复杂的生物行为。为促进医疗领域的高质量发展，推进临床技术创新发展，研发一类典型医

疗器械及临床植入物高性能生物功能表面的简便高效、切实可靠的制备方法势在必行[37]。近年来，已经发展出了诸多针对医用金属材料表面进行改性的方法，如表 2 所示[38-51]。这些研究方法都立足于调控植入物的耐蚀性及降解速率，阻断有害元素释放，促进植入物与生物组织力学性能适配，增加生物相容性及获得抗菌表面等。虽然目前的各类方法均已开展了较多研究，并且某些方法已经开始商业化应用，但便捷高效、绿色安全、参数可调可控、尽可能较少损伤医用金属材料基底的表面改性方法仍在探索中。激光表面改性可以控制植入物表面的精度特征，高效，无污染，材料消耗低，已被广泛应用于多种材料表面周期性微/纳米结构的制备，为金属材料的表面改性提供了新思路[52-53]。常见的微/纳米结构有激光诱导周期性表面结构(LIPSS)、纳米柱、纳米粒子(NPs)、微沟槽、微波纹[54]等。此外，激光改性方法还可以结合涂覆生物活性材料等方法来改变表面的相位结构和化学成分[55-57]。在目前的激光加工生物功能微结构技术中，纳秒(ns)激光[58]、飞秒(fs)激光[59]、紫外线(UV)激光[60]及准分子激光[61]等不同波长激光的应用均有报道。

表 2 医用金属材料的常规表面改性方法

Table 2 Conventional surface modification methods of biomedical metal materials

Method	Objective	Advantage	Inferiority	Ref.
Anodic oxidation	Form corrosion resistant protective film, blocking the release of harmful elements	Coating micropores are conducive to cell adhesion	The prepared film is generally rough and porous, with poor protective effect. It is generally necessary to seal the hole after oxidation	[38-39]
Micro arc oxidation	Adjust the dissolution rate, increase corrosion fatigue life	No pollution, low original surface requirements, can be completed in stages, without vacuum or low temperature conditions	High energy consumption and difficult processing in large area	[40-41]
Plasma spraying	Improve the ability of bone integration and endow the surface with antibacterial properties	High cost performance, mature process, wide selection of raw materials, and large-scale production	The equipment is expensive, the spraying rate is small, and the quality requirements of spraying materials are high	[42-43]
Ion implantation	Improve friction and wear properties, improve antibacterial and corrosion resistance, and regulate surface physical properties	No change in thickness, no physical condition requirements, wide range of applicable elements and strong parameter controllability	The equipment is complex and damages the original matrix lattice	[44-45]
Electrochemical deposition	Increase the physiological stability, cell surface activity, and surface antibacterial properties of implants	Various grain sizes can be obtained, the method is simple, the obtained nanocrystals have unique properties, the method has low cost and high efficiency	Electric burn, dark spot, gas stripe, crystalline attachment	[46-47]
Sol-gel	Increase biocompatibility	Homogeneous doping of multiple substances at the molecular level	The preparation time is long, small holes and cracks are easy to appear in drying	[48-49]

（续表）

Method	Objective	Advantage	Inferiority	Ref.
Friction stir treatment	Refine surface grains and increase corrosion resistance	Eliminate shrinkage porosity and shrinkage cavity defects, improve mechanical properties of materials, influence area is small	The travel end keyhole needs to be repaired	[50-51]

不同于长波长激光诱导分子振动引起热效应，飞秒激光由于脉宽极低，以较低的脉冲能量就可以获得极高的峰值功率，引发多光子吸收，从而达到材料去除的目的。飞秒激光加工过程中的热效应可以忽略（冷加工），可以实现微观结构的空间选择性操控[62]。作为微纳制造的最理想方法之一[63]，飞秒激光技术已被广泛应用于制备生物功能表面[64]。如图 2(a)所示，当飞秒激光辐照金属表面时，脉冲能量被自由电子系统吸收[65-66]。随后，由于金属中存在足够的自由电子，电子之间的碰撞导致它们在大约 100 fs 的时间尺度上热化。与轻质电子不同，重离子不能跟随电磁场快速振荡，因而不能直接吸收光辐射。电子与重离子通过碰撞传递能量。由于电子与重离子巨大的质量差，每次碰撞传递的能量有限，因此电子-声子耦合弛豫时间超过了电子或离子碰撞时间。电子系统与晶格之间的热力学平衡只有在多次的电子-声子耦合之后才能达到。受电子-声子耦合效率的影响，热平衡常常发生在皮秒或更大的时间尺度上[67]。飞秒激光能量迅速在聚焦区域沉积，导致材料内形成强烈的压应力，且脉冲持续时间或电子-晶格的弛豫时间少于材料膨胀所需的时间，材料内的压应力急剧增大[68]。光致压应力与材料表面相互作用在材料内产生拉应力波，使得材料出现孔洞。如若激光入射能量超过光机械散裂阈

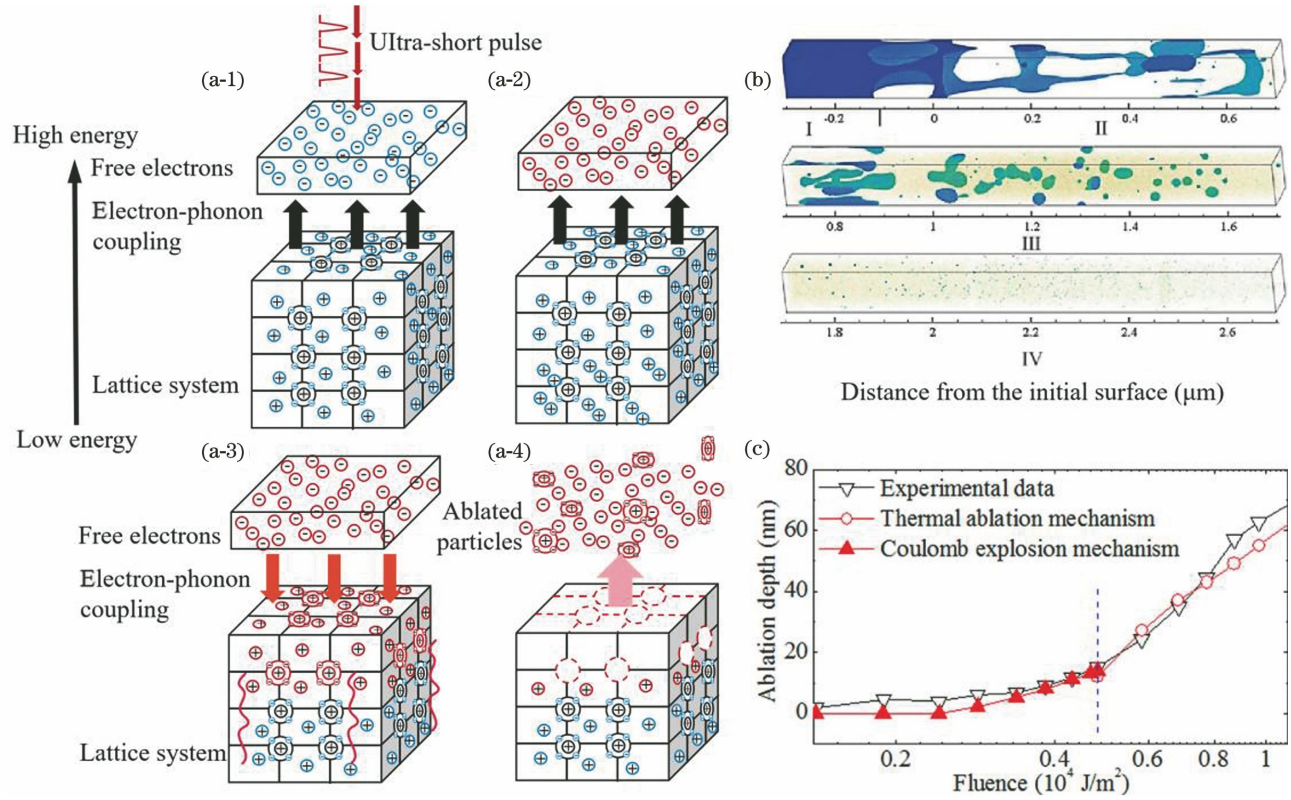

图 2 飞秒激光辐照金属表面。(a)电子-晶格能量传递[65]：(a-1)吸收，(a-2)热化，(a-3)能量传递，(a-4)烧蚀；(b)机械剥离[70]；(c)库仑爆炸[73]

Fig. 2 Femtosecond laser irradiating metal surface. (a) Electron lattice energy transfer[65]: (a-1) absorption, (a-2) heating, (a-3) energy transfer, (a-4) ablation; (b) mechanical stripping[70]; (c) Coulomb explosion[73]

值，则拉应力会使金属表面产生孔隙，导致一层或多层材料分离和喷溅，即光机械散裂[69-70]，如图 2(b)所示。随着激光能量增加，材料表面的热力学稳定状态被打破，材料爆炸性分解成液体和蒸气原子，即相爆炸[71]。相爆炸同时会导致等离子体羽流膨胀，羽流使得材料抛出。光机械散裂、相爆炸及等离子体羽流等同时交互作用，共同决定着飞秒激光处理后的表面形貌。此外，飞秒激光辐照材料表面，激发电子从表面逃逸，导致材料表面呈正电性，材料表层进而因库仑力排斥作用发生瓦解，造成材料剥离，如图 2(c)所示，此过程被称为库仑爆炸[72-73]。

因为飞秒激光与材料作用的时间极短，目前尚未发展出针对飞秒激光-材料相互作用的有效监测手段，不过近年来研究人员提出了诸如双温模型(TTM)、分子动力学(MD)等多种模拟手段[74]。图 3 展示了利用 TTM-MD 复合手段模拟脉宽为 100 fs 的激光照射铝表面的整体视觉图像，可以看出，微结构深度在激光光斑中心附近超过 200 nm，并随着到光斑中心距离的增加而减小[75]。光机械散裂及相爆炸以“镶嵌方法”引起材料喷溅[76]。不同飞秒激光参数条件下，电子-声子耦合带来的复杂的晶体温度分布，导致了材料表面的多种拓扑结构。

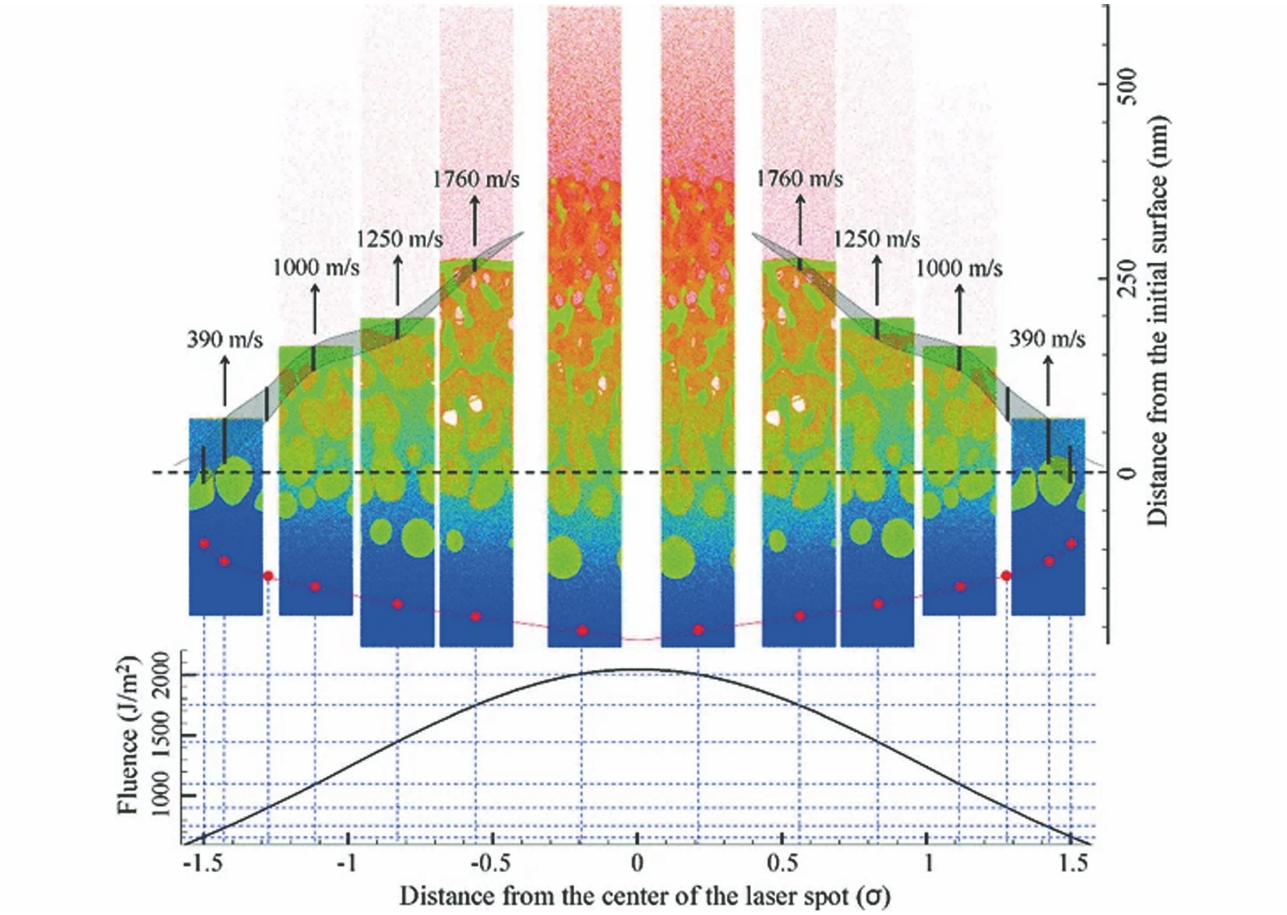

图 3 利用 TTM-MD 方法模拟 100 fs 脉宽激光脉冲照射铝目标材料喷溅的整体视觉图像[75]（原子依其势能着色，蓝色表示目标主体中的低能原子，红色表示气相原子，红线连接的红点标记了熔化峰的位置）

Fig. 3 TTM-MD method is used to simulate the overall visual image of Al target material splashing irradiated by 100 fs laser pulse[75] (the atoms are colored according to their potential energy. Blue represents low-energy atoms in the target body, red represents gas-phase atoms. The red dot connected by the red line marks the position of the melting front)

本文聚焦钛合金和镁合金生物金属材料基底，基于飞秒激光诱导具备临床生物医疗功能的微结构表面的研究现状，总结现有相关成果，并展望未来的发展趋势与主要研究方向。

2 飞秒激光制备钛合金高精度体液光谱检测衬底

人体体液中富含蛋白质、葡萄糖、核酸、神经递

质、氨基酸及病原微生物等人体健康信息，为评价机体健康状况提供了早期特异性指标[77]。体液检测常常因为标本被污染、送检不及时、采集不规范、标本凝固、容器错误等造成样品失效、检测不合格[78]。体液是高度复杂的液体环境，要求检测方法稳定、灵敏度及复现性高。光谱检测方法具有操作简单、响应迅速的特点。便携式光谱设备为体液检测提供了切实可靠的新方法。近红外光谱和傅里叶变换红外光谱检测方法易受水性环境干扰，而拉曼散射光谱检测方法的灵敏度较低，检测精度差[79]。

表面增强拉曼散射和表面增强荧光效应可以准确、灵敏地捕捉特征指纹信息[80]。目前的研究认为，表面增强拉曼散射和表面增强荧光效应一般发生在贵金属及碱金属等有限几种金属材料的粗糙化表面。相对成本高且粒子聚集较为随机的金、银等贵金属纳米粒子以及化学性质活泼的碱金属[81]，钛合金成为光谱检测衬底的理想选择。

2.1 基于表面增强拉曼散射的葡萄糖检测

表面增强拉曼散射(SERS)是通过吸附在金属纳米结构表面上的分子与金属表面发生等离子共振(SPR)相互作用而引起的拉曼散射强度增强的现象[82]，自 1974 年由英国南安普敦大学化学系 Fleischmann 等[83]发现以来，已被广泛应用于化学催化、生物医药、医疗成像诊断等领域[84-88]。SERS 因为能提供组分的特征指纹信息，在定量及定性分析中具有较大应用价值[89]。SERS 的增强因子(EFs)高达 $10^{14}\sim10^{15}$，这使得 SERS 识别位于纳米颗粒表面或两个颗粒连接处的单个分子成为可能[90]。研究人员普遍认为，只有同时满足特定金属种类及特定粗糙化表面这两个条件的衬底才具备 SERS 所必需的“热点”。如图 4 所示，“热点”是指空间狭小的区域，如纳米尺寸的尖端、纳米颗粒之间的小间隙、纳米颗粒与衬底之间的缝隙。间隔 2 nm 的银纳米球二聚体，其热点面积不足总面积的 1%，但其贡献的 SERS 信号强度占总强度的 50%以上(假设粒子均匀分布)[91]。换言之，只要一个纳米粒子进入“热点”就会被检测，这决定了 SERS 的高灵敏度。

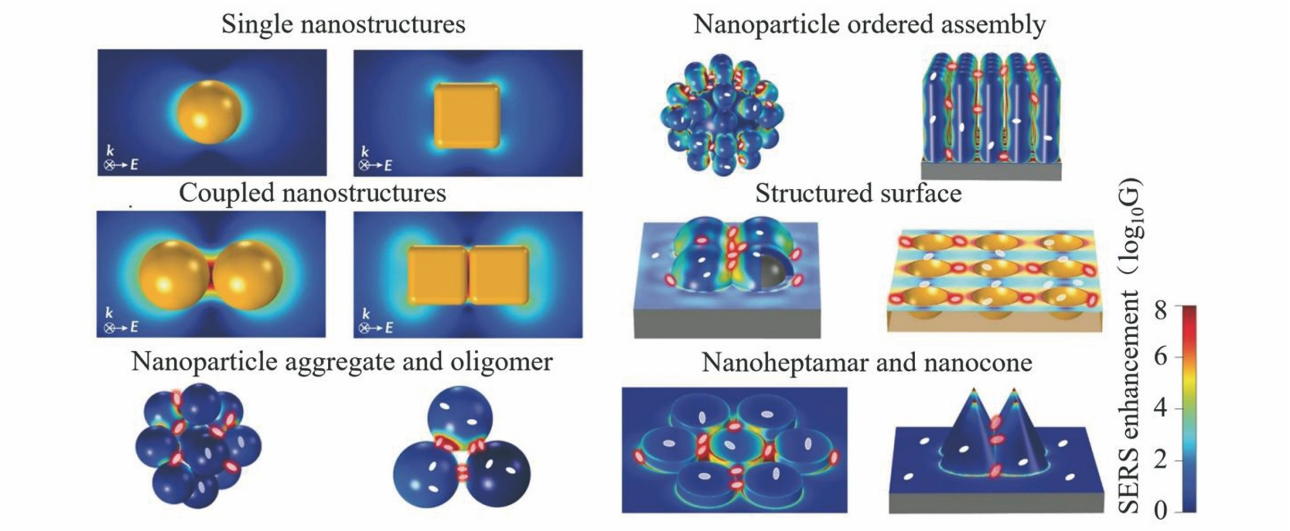

图 4 典型金纳米粒子结构中 SERS 强度分布的有限元模拟[91]

Fig. 4 Finite element simulation of SERS intensity distribution in typical Au nanoparticle structure[91]

研究表明，电磁增强(EM)和化学增强(CM)是引发 SERS 现象的两个主要机理[92]，其中：电磁增强为长程作用，它可以影响到距离金属表面约几十纳米的范围；化学增强是一种短程作用，通常发生在第一吸附分子层上。如图 5(a)所示，电磁增强现象认为，金属衬底中的电子可以看成是均匀正电荷背景下运动的电子气体，当电磁波照射微结构金属表面时，微结构诱导电磁波形成电磁振荡，激发衬底表面产生 SPR 现象，金属表面电场增强激发近基底表面分子发生强拉曼散射[93-94]。如图 5(b)所示，化学增强现象认为，当光场作用于金属衬底表面时，光致电荷转移，随后电子-空穴对的复合产生电子共振，使得分子的有效极化率大幅增大，从而增强拉曼散射[95]。

目前，制备 SERS 功能表面的方法主要有化学自组装[96]、纳米粒子修饰[97]、深紫外光刻[98]、氩离子溅射[99]等。飞秒激光诱导衬底表面周期性结构较之其他方法操作简单，周期较短，易于实现大面积制备，近年来吸引了较多关注。Xu 等[100]利用飞秒激光诱导等离子体辅助消融(LIPAA)制备了表面

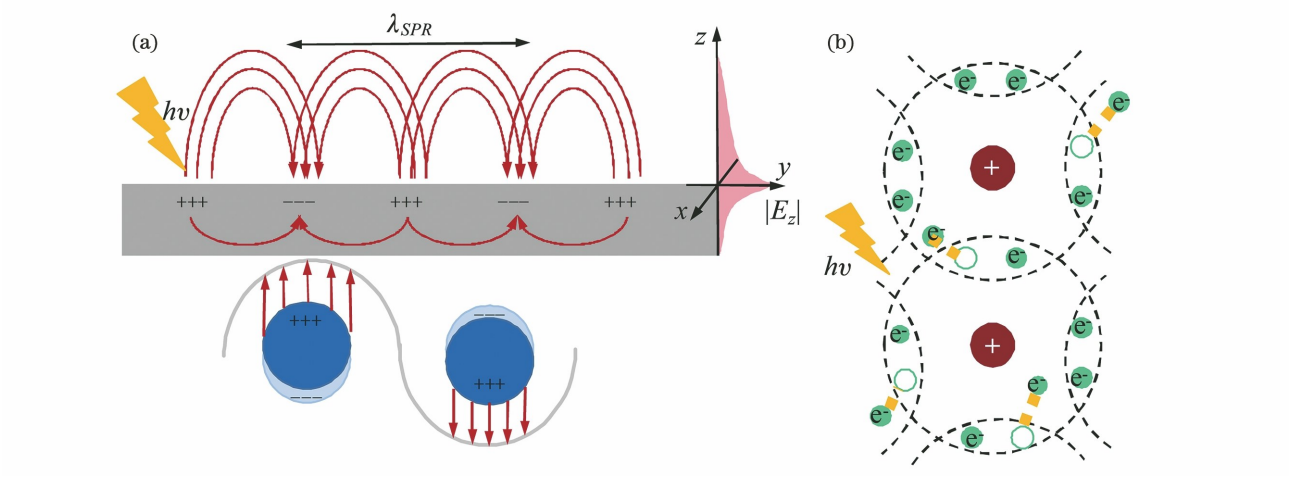

图 5 引发 SERS 现象的电磁增强和化学增强机理示意图。(a)电磁增强机理;(b)化学增强机理

Fig. 5 SERS phenomenon caused by electromagnetic enhancement and chemical enhancement mechanisms. (a) Electromagnetic enhancement mechanism; (b) chemical enhancement mechanism

微结构,通过调控银和金纳米粒子的表面形态、大小及分布,可将其用于农作物农药残留的现场检测。Luo 等[101]利用激光直写在氩气氛围下制备了周期性微凹坑阵列,它可用于检测孔雀石绿、结晶紫及苏丹红等食品添加剂的含量。葡萄糖是反映人体血糖含量的重要指标,其在血液、尿液中的含量是心血管等疾病重要的筛查及治疗依据。便捷准确的葡萄糖检测方法在临床诊断与治疗中具有重要意义。在目前的研究中已经发展出了比色法[102]、电化学法[103]、光谱检测法[104]等,其中的光谱检测法因为灵敏度及分辨率高、检测极限(LOD)低、检测过程更为便捷而吸引了较多研究人员关注[105]。崔智铨等[106]利用飞秒激光在钛合金 TC4 表面制备了镀银 LIPSS,制备过程如图 6(a)所示。该衬底对葡萄糖的检测极限为 10^{-7} mol/L,在 10^{-7}~10^{-3} mol/L 范围内葡萄糖浓度与拉曼强度呈良好的线性关系。

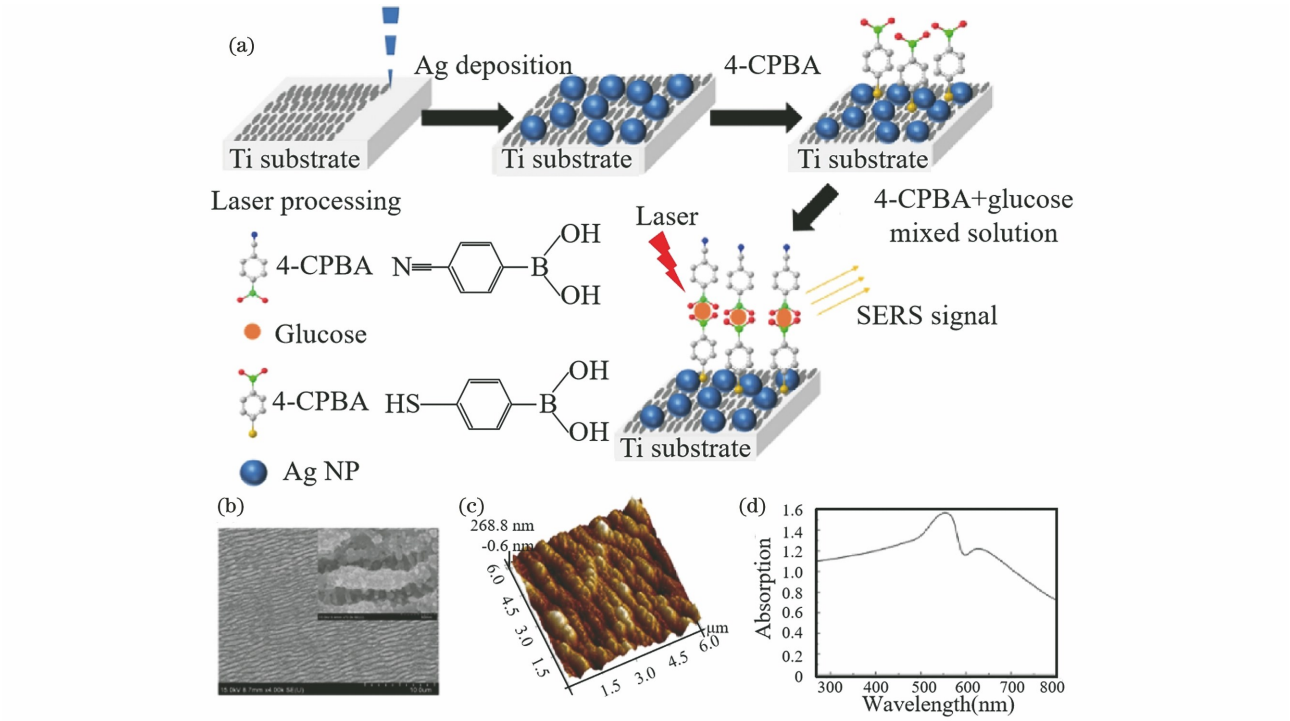

图 6 飞秒激光制备 SERS 衬底[106]。(a)制作流程示意图;(b)镀银衬底的扫描电子显微镜(SEM)图像;(c)镀银 LIPSS 表面的原子力显微镜(AFM)图像;(d)镀银 LIPSS 表面的吸收光谱

Fig. 6 Femtosecond laser processing SERS substrate[106]. (a) Schematic of manufacturing process; (b) SEM image of silver plated substrate; (c) AFM image of silver plated LIPSS surface; (d) absorption spectrum of silver plated LIPSS surface

此外，崔智铨等[106]还针对人尿液样品中葡萄糖的SERS检测进行了研究，结果与临床实践吻合良好。该研究为生产结构可控的用于葡萄糖检测的SERS衬底提供了一种简便方法。

2.2 基于表面增强荧光效应的蛋白检测

表面增强荧光效应(SEF)是指当荧光物质靠近金属纳米结构衬底附近时，其辐射行为将受到调控，在适当的条件下，荧光物质的光谱辐射强度相对于自由态强度有所增加。光激发电场 E_e 某时刻的状态可由图7(a)中的正弦曲线表示，该电场诱导表面电子振荡，形成表面等离子体激元(SPPs)，即沿着金属介质界面传输的电磁辐射波，如图7(a)中的 E_{SPPs} 所示。SPPs可以有效诱导衬底表面荧光分子的电子跃迁，从而产生荧光增强信号，如图7(b)所示。制备周期性结构表面是调控荧光信号增强的有效手段[107-108]。在可激发SEF现象的周期结构的制备方面，目前人们已经开发出自组装、磁控溅射、化学刻蚀等方法[109-110]。

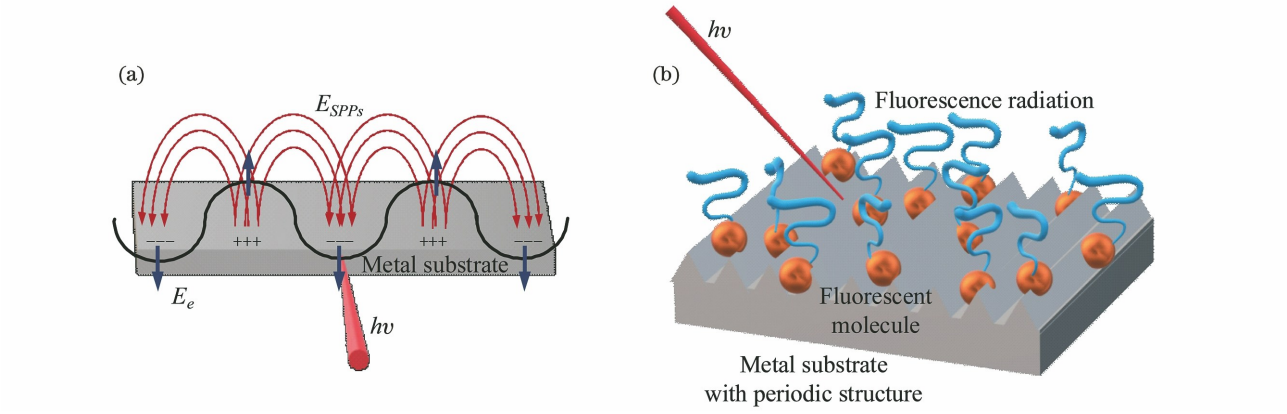

图7 金属表面荧光的增强机制。(a)等离子体振荡场；(b)SPP调控分子荧光辐射示意图

Fig. 7 Enhancement mechanism of metal surface fluorescence. (a) Plasma oscillation field; (b) fluorescence radiation of SPP regulated molecules

作为一种新兴技术，自组装技术的可重复性和应用范围有待进一步提高，比如，磁控溅射技术对真空条件、设备状况、操作技术等的要求较为严苛[111]，不便于大范围推广。因此，开发一种操作简单、复现性强的周期表面结构制造技术的需求日趋旺盛。血清蛋白是血液循环系统中重要的蛋白质，主要在肝脏中合成，是新陈代谢产物的主要载体，具有维持血液胶体渗透压的功能[112]，并可作为自由基捕获剂。张佳茹等[113]采用飞秒激光在TC4钛合金基材上诱导分层周期性表面结构，以此来增强牛血清白蛋白(BSA)荧光检测。该分层周期性表面结构包括微槽、亚微米LIPSS和纳米粒子。可用于有效激发SPPs的光栅周期必须是SPPs波长的整数倍，在张佳茹等的研究中，SPPs波长为203.29 nm，制备的LIPSS的周期为812 nm(是SPP波长的3.99倍)，如图8所示。考虑到LIPSS的测量误差，认为光栅周期为SPP波长的4倍，因此该LIPSS表面在SEF检测中具有较高的灵敏度。采用LIPSS表面检测BSA中 Cu^{2+} 的浓度，结果显示，荧光强度与 Cu^{2+} 浓度呈线性关系[113]。

2.3 基于拉曼散射-荧光双增强(SERS-SEF)的葡萄糖检测

表面增强拉曼散射(SERS)和表面增强荧光(SEF)的整合极有可能提高生物医学领域光谱研究的灵敏度和可重复性。Kamalieva等[114]开发了一种基于银纳米粒子和硅保护薄膜(AgNPs/Si)的SERS/SEF双增强基底，氰化物在该复合结构上的拉曼散射和荧光信号增强因子分别为10和40，低于单一功能基底。Cao等[115]利用鱼皮明胶($HAuCl_4 \cdot 4H_2O$)与纳米金群落(AuNCs)形成壳结构来实现SERS/SEF双增强，拉曼和荧光信号的增强因子分别为 3.1×10^4 和4。此外，Cyrankiewicz等[116]研究了SERS银纳米粒子和金属增强荧光(MEF)的增强特性，他们发现，“热点”的聚集是高效SERS的先决条件。Chang等[117]在研究中发现，金属颗粒的聚集状态以及金属结构与发射物之间的间隔对增强比有很大影响。SERS/SEF双增强集成于同一衬底虽然吸引了较多关注，但几乎所有的双增强衬底都是金属纳米粒子。此类衬底的主要缺点是金属纳米粒子的聚合导致所制备样品的复现性差。此外，纳米粒子的制备过程非常复杂，其生物相容性有待进一步改进，从而极大地限制了SERS/SEF双增强衬底在生物医学中的实际应用。为解决此问题，卢立斌等[118]采用飞秒激光直接在钛合金TC4衬底上制备出由NPs、

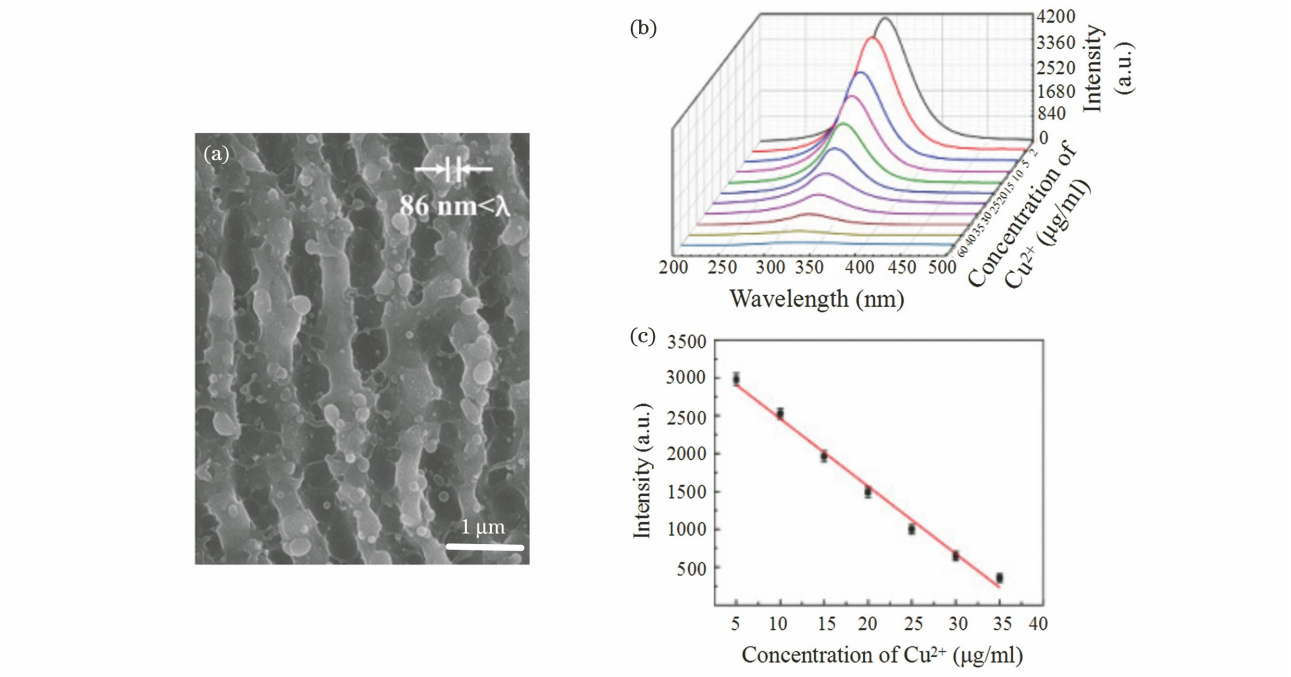

图 8 SEF 衬底的微观形貌与荧光光谱[113]。(a)飞秒激光诱导分层 LIPSS;(b)不同 Cu^{2+} 浓度下的荧光光谱;(c)光谱强度与 Cu^{2+} 浓度呈线性关系

Fig. 8 Microstructure and fluorescence spectra of SEF substrate[113]. (a) Femtosecond laser induced layered LIPSS; (b) fluorescence spectra under different Cu^{2+} concentrations; (c) linear relationship between spectral intensity and Cu^{2+} concentration

LIPSS 和微沟槽组成的复合 LIPSS 结构,获得了 SERS-SEF 双增强衬底。荧光增强的快速定位追踪能力结合拉曼增强的选区检测能力,使得该衬底可以实现光谱增强的多目标识别检测,提高了分析精度和分析质量。如图 9 所示,卢立斌等采用该 SERS-SEF 双增强衬底对结晶紫(CV)乙醇溶液进行检测后发现,拉曼及荧光增强因子分别为 7.85×10^5 和 14.32。利用该衬底对葡萄糖进行检测,检测极限达到 14.4 mol/L,证明了该衬底在糖尿病检测中的应用潜力。

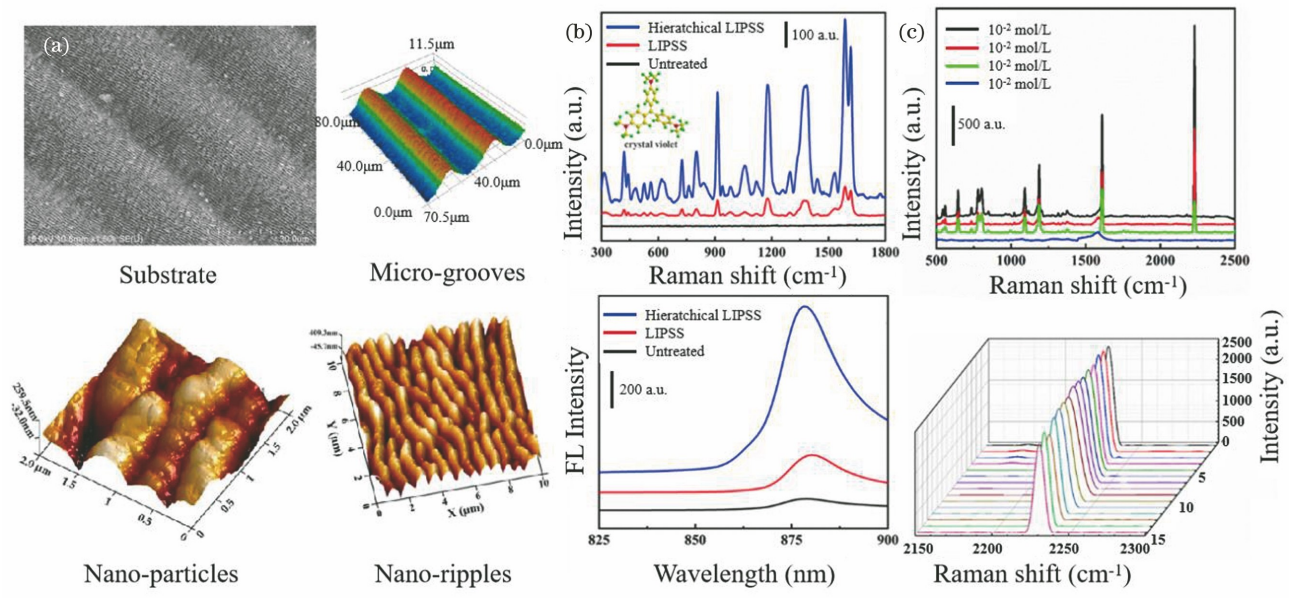

图 9 双增强衬底的微观形貌与光谱检测[118]。(a)SERS-SEF 衬底的形貌;(b)拉曼光谱和荧光光谱;(c)葡萄糖检测

Fig. 9 Microstructure and spectral detection of double reinforced substrates[118]. (a) Morphology of SERS-SEF substrate; (b) Raman and fluorescence spectra; (c) glucose detection

3 飞秒激光制备镁合金植入物微纳表面调控细胞行为

材料表面的形态特征是影响植入物表面细胞行为的重要因素，直接关系着后续细胞增殖和成骨分化[119]。研究认为，相对于光滑表面，植入物表面具有微纳结构时更有利于实现细胞行为的调控[120]。微纳结构对细胞行为的影响机理在于其对早期蛋白吸附、细胞黏附及后续的细胞伸展、增殖、分化等一系列生物学行为的调控[121]。若植入物表面的微结构尺寸接近细胞的大小，就会对植入物表面的细胞活力和迁移产生积极影响[122]。

3.1 微结构表面影响细胞黏附

细胞与基底接触数秒就会发生蛋白质吸附效应，如图 10(a)所示。蛋白质吸附主要有朗谬尔模型、简单粒子模型、扩散粒子模型等[123]，其吸附主要依靠静电[124]、表面润湿性[125]、共价键作用[126]等，具体情况与基底的表面形貌、理化性能、溶液条件等关系紧密[127]。如图 10(b)所示，细胞外基质蛋白在基底表面吸附，并形成牢固附着物，促使细胞吸附。研究表明，细胞几乎只对基底微纳米级形貌结构作出反应[128]。目前，在细胞和亚细胞尺度上的多种表面图案化技术，例如化学蚀刻、静电纺丝、电化学沉积以及微弧氧化等[129-131]，已被公开报道。由于可以通过简单地改变激光加工参数在微尺度或纳米尺度上修饰形貌，并且在辐照过程中不引入细胞毒性物质[132]，飞秒激光已被成功用于表面修饰，从而控制细胞的行为[133]。

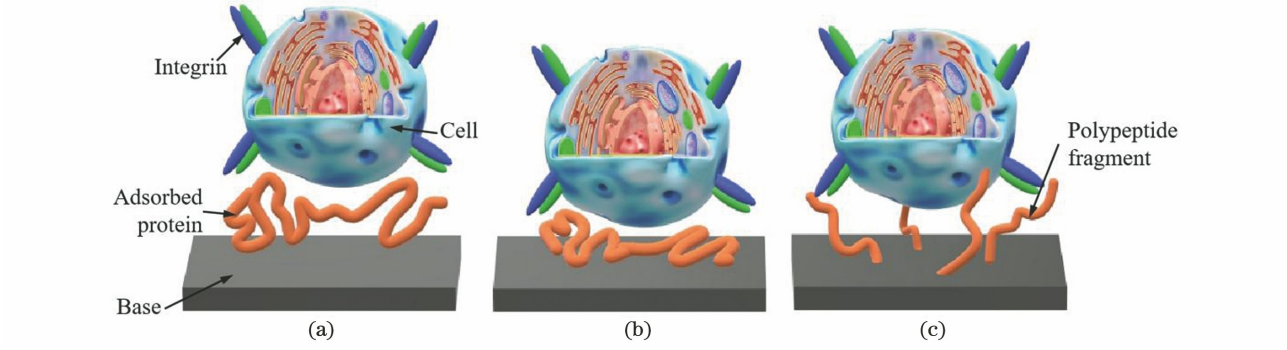

图 10 细胞在基底上的黏附行为。(a)蛋白质吸附；(b)细胞外基质蛋白沉积；(c)工程化黏附

Fig. 10 Adhesion behavior of cells on base. (a) Protein adsorption; (b) extracellular matrix protein deposition; (c) engineering adhesion

Czyż 等[134]使用双通道 Nd∶YAG 激光制备了周期约为 200 nm 的线性结构，该结构可以用来控制平滑肌细胞的生长方向。Kennedy 等[135]发现，具有不同微结构的基底可以控制细胞的密度、大小，并能拉长细胞的形状。Dumas 等[136]使用飞秒激光在 Ti-6Al-4V 合金上制备了周期约为 40 μm 的微波纹，并证明了所有经过激光处理的表面都会强烈抑制与脂肪相关的基因（*PPARγ2*，*C/EBPα*）的表达，同时可以调节与骨质相关的基因（*RUNX2*，骨钙素）的表达。张佳茹等[137]在对 Mg-6Gd-0.6Ca 合金基底进行连续激光重熔后，利用飞秒激光在表面诱导 LIPSS 及微沟槽结构，然后将得到的生物功能基底进行小鼠成骨细胞（MC3T3-E1）培养实验，培养 48 h 细胞的荧光图像如图 11 所示。初始表面由于存在大量氢气孔，极不利于细胞附着；在重熔表面，细胞无规则排列，而且细胞扩展，外延形状不规则；在激光重熔＋LIPSS 表面，细胞附着形态倾向于细长形，这是因为在细胞骨架重组过程中，LIPSS 可以向细胞提供各向异性和持久的机械刺激，导致细胞形状各向异性[138]；激光重熔＋微沟槽结构破坏了重熔层的完整性，微沟槽区的耐蚀性降低，再次出现氢气孔，细胞主要黏附在沟槽间的重熔区[137]。

3.2 微结构表面调控细胞迁移

细胞迁移是指细胞在基底表面附着后的爬行行为，是细胞发育和分化的关键现象。细胞迁移基本上由图 12 所示的伪足延伸、新黏附建立、胞体尾部收缩等步骤在时空上交替完成，是高等生物伤口愈合、血液凝固、免疫应答、组织发育等多种生命活动的重要支撑[139]。

Martínez-Calderon 等[140]利用飞秒激光加工出了由宽 30 μm 和 10 μm 的微条纹组成的总周期为 40 μm 的复合周期性结构，并且在两种宽度条纹内分别诱导 LIPSS 结构。在其表面培养人体间充质干细胞（hMSCs）后发现，细胞形态受到微结构特定方向的影响，除细胞端部尖化外，观察不到细小的丝状体，细胞在拉伸、结合和收缩后沿着微通道迁移。

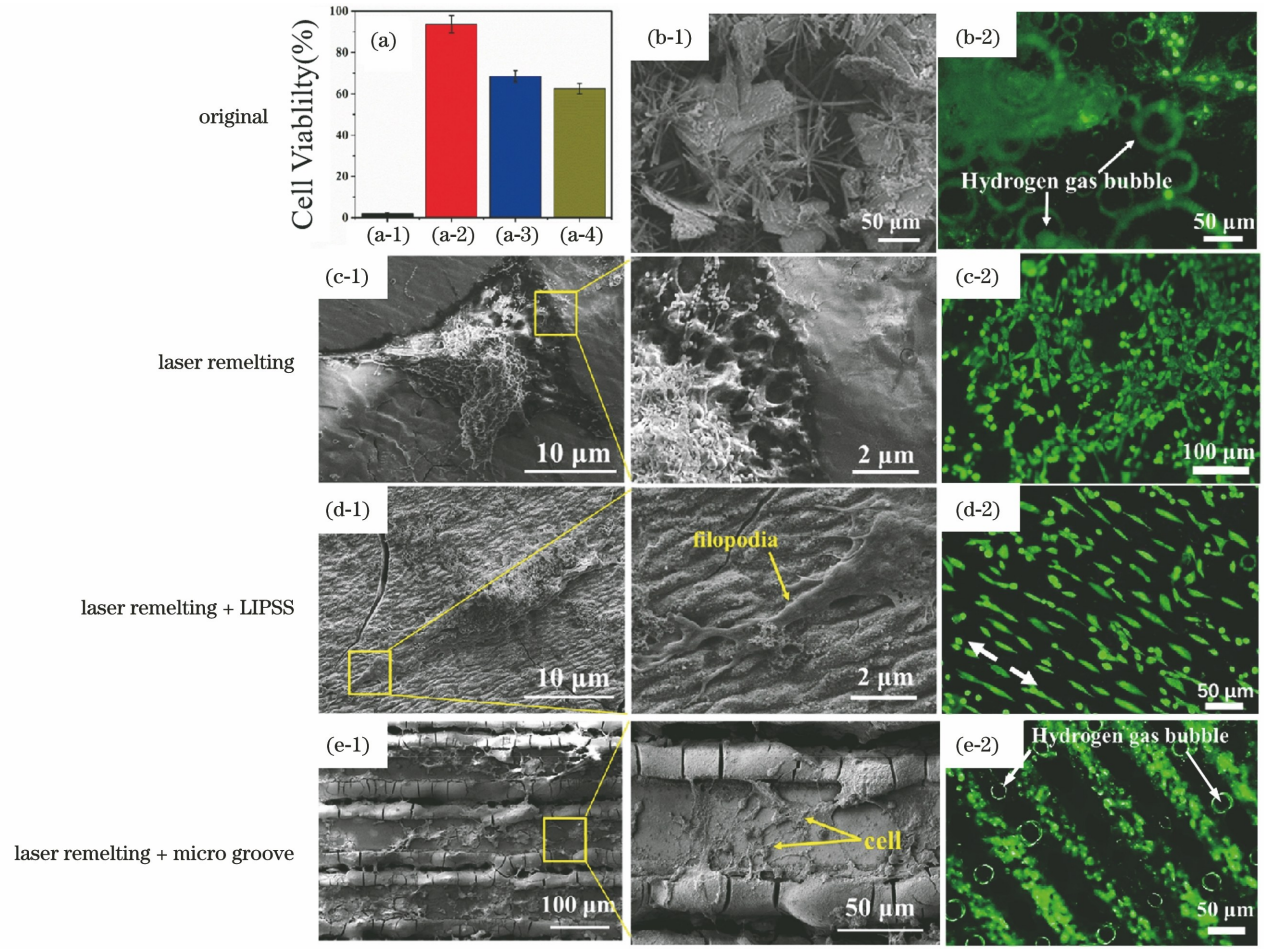

图 11 不同状态 Mg-6Gd-0.6Ca 合金表面培养 MC3T3-E1 细胞的活性以及细胞黏附的 SEM 图像和荧光图像[137]，其中(a-1)为原始表面，(a-2)为激光重熔表面，(a-3)为激光重熔＋LIPSS 表面，(a-4)为激光重熔＋微沟槽表面

Fig. 11 Cell activity of MC3T3-E1 cultured on Mg-6Gd-0.6Ca alloy with different states and cell adhesion SEM and fluorescence images[137], where (a-1) represents original surface, (a-2) represents laser remelting surface, (a-3) represents laser remelting + LIPSS surface, and (a-4) represents laser remelting + micro groove surface

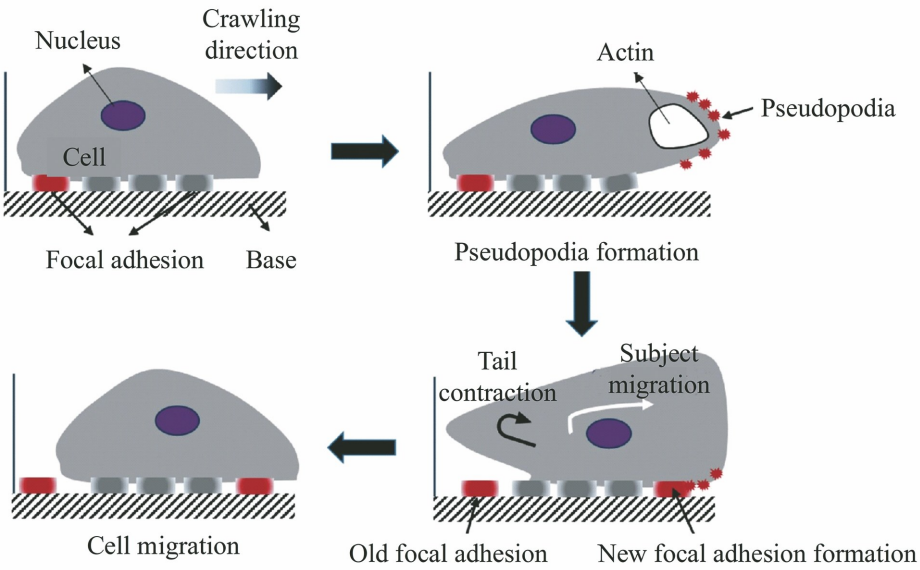

图 12 细胞迁移过程示意[139]

Fig. 12 Schematic of cell migration process[139]

这表明飞秒激光诱导表面微结构可以改善骨整合。Nuutinen 等[141]利用飞秒激光诱导一维与二维微结构，然后在其表面培养人骨肉瘤细胞(U-2 OS)，结果显示，周期性微沟槽结构极大地改变了细胞的形态和迁移行为。张佳茹等[142]利用中心波长为 1064 nm、波长为 800 fs、频率为 400 kHz 的飞秒激光，在连续波激光重熔稀土镁合金表面制备了如图 13(a)、(b)所示的周期为 865 nm、高度为 200 nm 的 LIPSS 结构。原始表面、激光重熔表面及激光重熔＋LIPSS 表面培养 MC3T3-E1 细胞 48 h 后的细胞 SEM 图像及荧光图像如图 13 所示。原始表面上未观察到细胞附着；如图 13(d)所示，细胞呈现具有不规则边界的板状，并且倾向于各向同性迁移，在激光重熔表面上形成了可忽略的丝孔；如图 13(e)所示，细胞在激光重熔＋LIPSS 表面上的扩散是各向异性的，细胞的前沿被拉伸，生长出更多的丝状足，证明了 LIPSS 结构可以调控细胞的定向迁移。

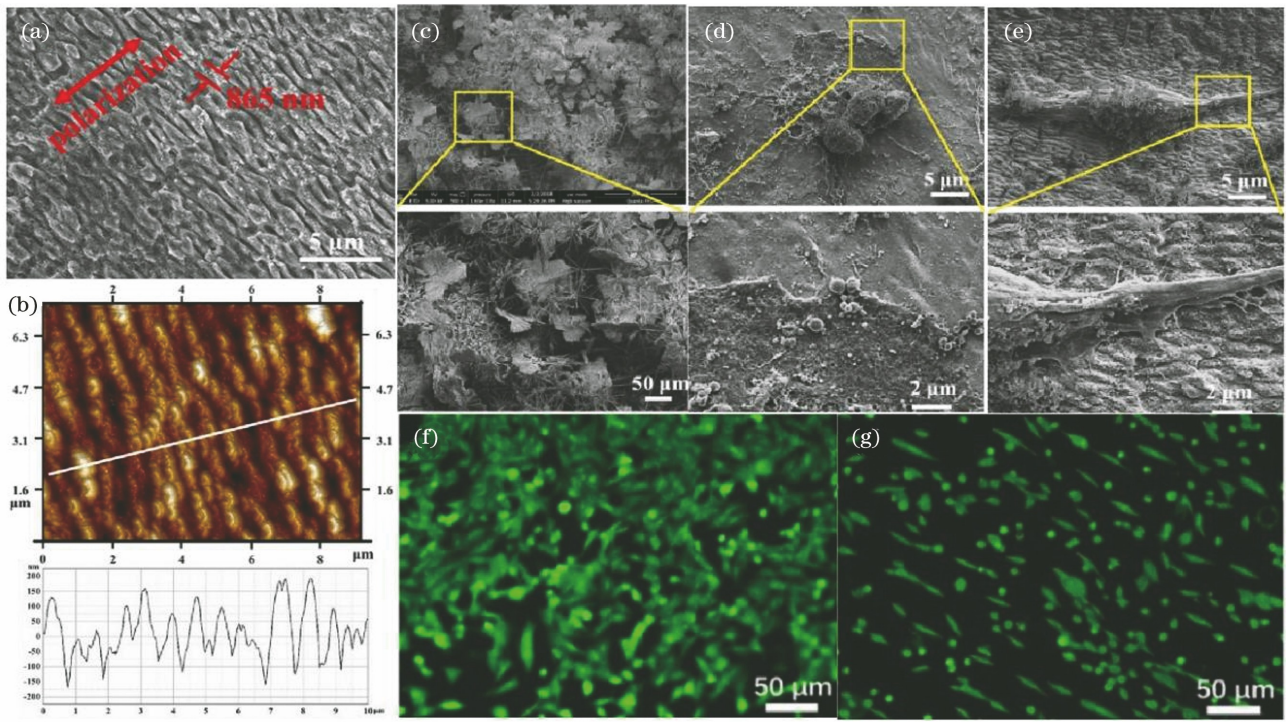

图 13 LIPSS 调控细胞迁移[142]。(a)～(b)LIPSS 的周期及高度；(c)～(e)培养 48 h 后原始表面、激光重熔表面、激光重熔＋LIPSS 表面的细胞迁移行为；(f)～(g)培养 48 h 后激光重熔表面和激光重熔＋LIPSS 表面的细胞荧光图像

Fig. 13 LIPSS regulates cells migration[142]. (a)-(b) Cycle and height of LIPSS; (c)-(e) cell migration behavior on original surface, laser remelting surface, laser remelting ＋ LIPSS surface after 48 h culture; (f)-(g) cell fluorescence images of laser remelting surface and laser remelting ＋ LIPSS surface after 48 h culture

3.3 微结构表面促进细胞增殖分化

医疗植入物植入后，会发生细胞吸附与迁移，并会建立粘连和一系列生物力学、生化刺激，触发一系列细胞信号，导致细胞核调节基因表达，决定细胞增殖与分化。其中，微纳结构引导细胞骨架的信号，对后续细胞增殖与分化意义重大[143]。Takayama 等[144]发现飞秒激光制造的微型通孔及陨石坑状阵列结构可以增强小鼠成肌细胞 C2C12 的黏附力，加速细胞增殖和分化。Cunha[145]利用 Yb∶KYW 系统发射的中心波长为 1030 nm、脉冲时间为 500 fs 的飞秒激光直写了 LIPSS 及 NPs 结构，用该结构培养 hMSCs 四周后发现，LIPSS 和 NPs 的存在促进了基质矿化和骨样结节的形成，从而促进了成骨分化。马程鹏等[146]利用激光对 Mg-Gd-Ca 合金表面进行修饰，然后用其进行 MC3T3-E1 体外细胞培养实验；实验结果表明，MC3T3-E1 细胞在激光修饰标本表面存活良好，并且相较于原始表面的黏附性能、扩散性能和增殖能力等显著改善。梁春永等[147]利用能量密度分别为 0.127、0.64、1.27 J/cm^2，脉宽为 50 fs，中心波长为 800 nm 的飞秒激光，以 0.8 mm/s 的速度扫描 AZ31B 镁合金表面，分别制备出周期条纹、微孔洞与周期条纹混合结构以及无规律沟槽和颗粒混合结构，培养 MC3T3-E1 一周后发现，能量密度为 0.64 J/cm^2 时制备的微孔洞与周期条纹混合

结构的细胞增殖情况最好，如图 14 所示。

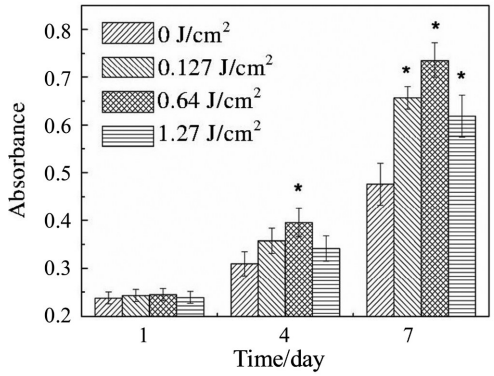

图 14 培养一周后 MC3T3-E1 的增殖情况（$p<0.05$ 时认为具有显著差异）[147]

Fig. 14 Proliferation of MC3T3-E1 cultured for one week (significant difference when $p<0.05$)[147]

4 飞秒激光制备口腔钛植入物抗菌功能表面

为解决口腔钛植入物表面细菌感染的问题[148]，研究人员采用多种方法来提高抗菌性能，如喷涂载药涂层[149]、添加重金属元素[150]、制备微纳结构[151]。研究发现，微纳结构在实现抗菌功能的同时不会产生细胞毒性，并能够提供接近天然骨的结构，促进细胞附着、分化和成熟。植入物抗菌表面的制备主要有涂覆涂层以及制备微结构两种思路。随着时间推移，涂层释放抗菌物质浓度下降。微结构抗菌效果较之涂层更为持久和稳定[152]。在微结构的制备方法中，等离子体加工很难预测准确的结构，而化学蚀刻容易导致表面损坏[153]，因此飞秒激光加工成为新兴选择。

4.1 微结构表面-细菌相互作用机理

微结构实现抗菌功能的机理目前普遍认为是细菌与微结构接触/悬挂的相互作用导致胞体破裂，以及表面超疏水抑制菌群生物膜形成。微结构表面的抗菌机理可以用图 15 所示的生物物理模型来解释。与微结构相互作用时，细菌细胞壁可以划分成两个区域：与微结构接触的区域以及悬挂于微结构之间的区域。Pogodin 等[154]制备的仿生蝉翼上的纳米

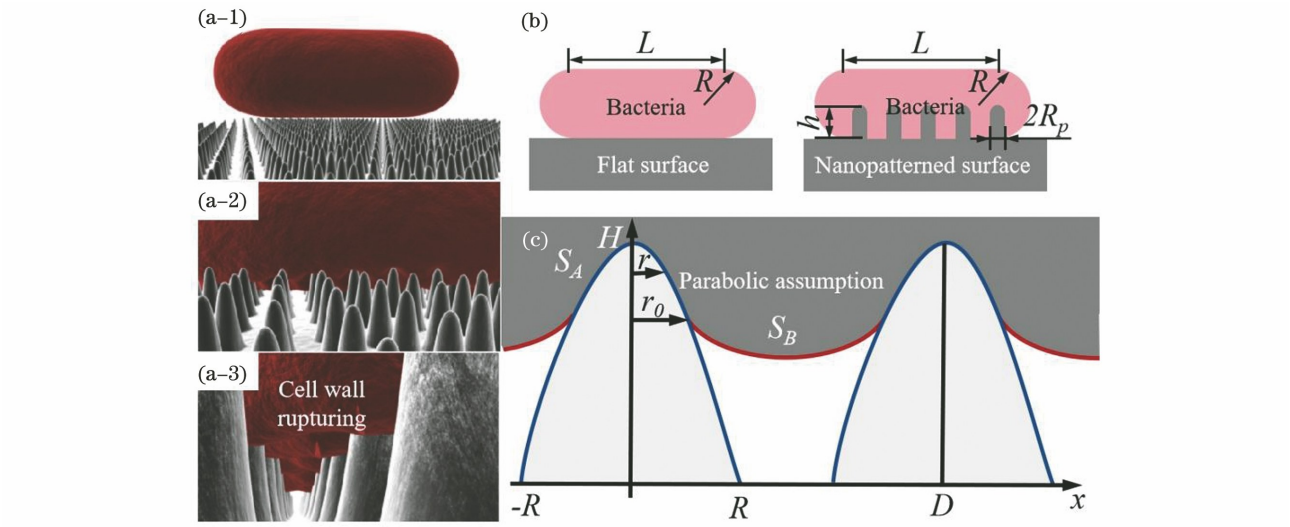

图 15 微结构与细菌相互作用。(a)细菌与微结构相互作用三维示意图[154]，其中(a-1)表示细菌接触微结构表面，(a-2)表示细菌吸附至微结构表面，(a-3)表示细菌细胞壁破裂；(b)细菌黏附在平坦表面和微结构表面[155]，其中 L 和 R 分别表示细菌的长度和半径，h 是纳米柱高度，R_p 是纳米柱半径；(c)细菌黏附在两个相邻“纳米岭”上[156]，其中，H 是“纳米岭”的高度，$2R$ 是“纳米岭”底部的宽度，S_A 表示“纳米岭”与细菌接触区域，S_B 表示细菌悬挂面积，r_0 是 S_A 与 S_B 分界线到 x 轴的距离，D 是两个相邻“纳米岭”之间的距离

Fig. 15 Interaction between microstructure and bacteria. (a) Three dimensional diagrams of interaction between bacteria and microstructure[154], where (a-1) represents bacteria contact the surface of microstructure, (a-2) represents bacteria adsorb to the surface of microstructure, and (a-3) presents rupture of the bacterial cell wall; (b) bacteria adhere to flat surface and microstructure surface[155], where L and R represent the length and radius of bacteria, respectively, h is the height of nano column, and R_p is the radius of nano column; (c) schematic of bacteria adhering to two adjacent “nano ridges”[156], where H is the height of “nano ridge”, $2R$ is the bottom width of “nano ridge”, S_A represents contact area between “nano ridge” and bacteria, S_B represents the area of bacteria hanging, r_0 is the distance from the boundary between S_A and S_B to the x-axis, and D is the distance between two adjacent “nano ridges”

柱尺寸(100 nm)比细菌细胞壁(10 nm)的厚度大一个数量级,忽略纳米柱之间细菌表面的曲率,可将细菌细胞假设成一个薄弹性层。由于微结构的存在,细菌膜通过增加相互作用的表面积吸附在多个纳米柱上,这易导致细胞壁拉伸不均匀,进而破裂。Li 等[155]考虑到细菌细胞自由能的变化,利用定量热力学模型研究了纳米结构表面的抗菌机理,图 15(b)显示了细菌细胞壁与平坦表面、纳米柱结构表面相互作用的差异。Li 等认为其差异主要在于细菌黏附的接触面积和黏附区域中细胞膜的变形。与平坦表面相比,纳米柱结构表面的抗菌效果较好,这主要归因于黏附面积的增加增强了膜的拉伸应变,当拉伸足够大时细胞溶解。因此,可以通过增加纳米柱高度与宽度来提升抗菌效果。这为抗菌微结构表面的制备提供了有益参考。类似地,Xue 等[156]假设与微结构接触的细菌膜以及悬挂在微结构之间的细菌膜变形成抛物线状,并在细胞壁的破裂中引入了重力和范德瓦耳斯力的联合作用。上述讨论均倾向于具有大间距、尖锐特征的微结构可以提高抗菌效果,而 Kelleher 等[157]则认为紧密的纳米结构更有利于提高抗黏附效率。

由于细菌更倾向于在亲水表面形成群落或生物膜,因此调节表面的润湿性能也是制备抑菌表面的重要方法[158]。Li 等[159]使用热液法在 AZ31B 镁合金上成功制备了羟基磷灰石(HA)/苯酸超疏水复合涂层,该复合涂层的水接触角为 152.52°,可以显著抑制大肠杆菌(*E. coli*)和金黄色葡萄球菌(*S. aureus*)的早期黏附和生长。Hizal 等[160]利用阳极氧化在铝基板上制备了纳米孔和纳米柱结构,并借助涂层使其具备亲水性或疏水性。由图 16 可以发现,相对于亲水表面,超疏水表面具有流体剪切效应及空气层截留作用,对 *S. aureus* 和 *E. coli* 的抑制率分别超过 99.9%和 99.4%,具有极佳的抗细菌黏附效果。

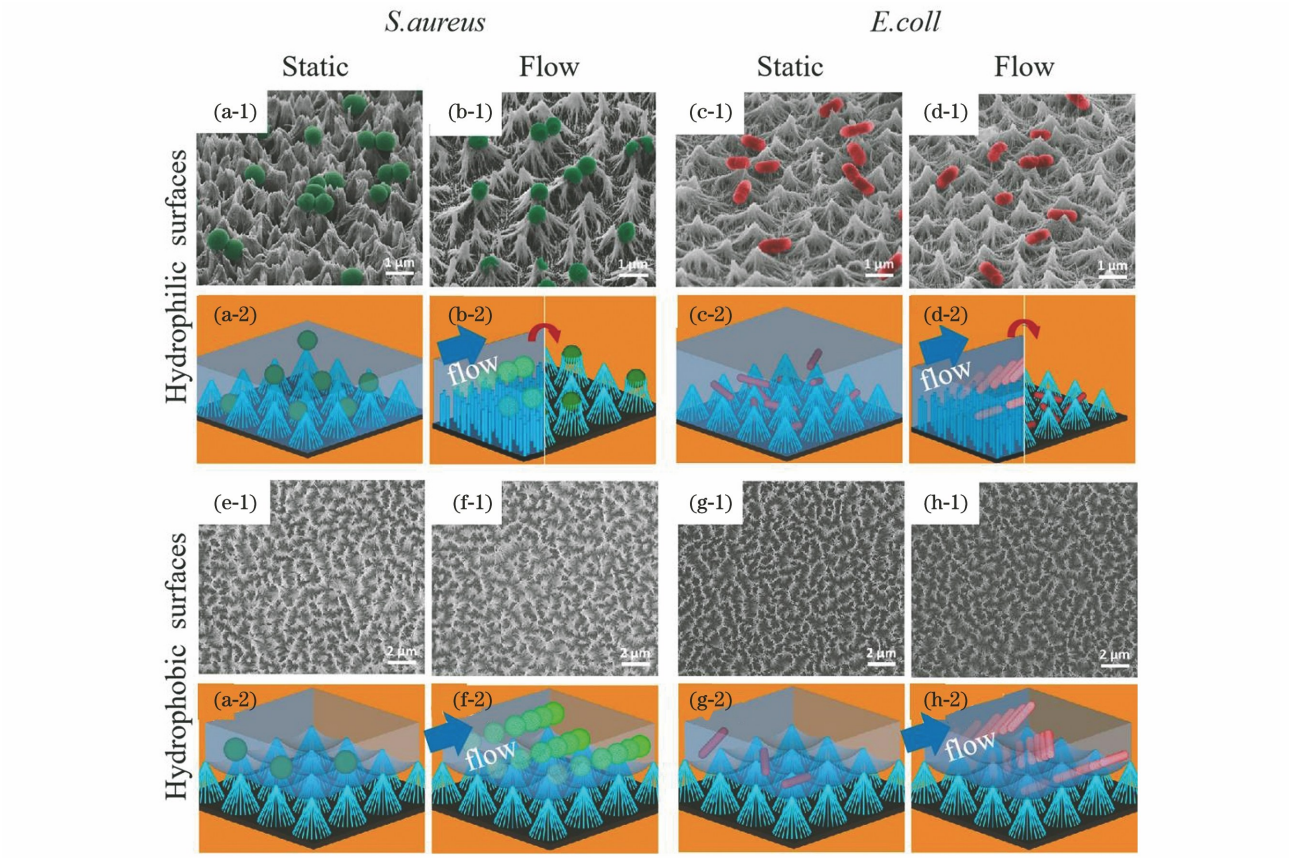

图 16 培养 24 h 后,*S. aureus* 与 *E. coli* 分别在亲水、疏水铝基板表面静态附着和动态附着的 SEM 图像及示意图[160]

Fig. 16 SEM images and schematics of *S. aureus* and *E. coli* static and dynamic adhesion on hydrophilic and hydrophobic aluminum substrate surfaces after 24 h culture[160]

4.2 飞秒激光制备抗菌钛合金微结构表面

在制备口腔钛植入物抗菌功能表面方面,王瑞等[161]利用飞秒激光掺银改性技术对牙种植体种植材料 TC4 表面进行改性,结果发现,随着蒸馏镀银层增厚,表面牙龈卟啉单胞菌(*P. gingivalis*)的附着减少。Cunha 等[162]利用 Yb∶KYW 产生

的中心波长为 1030 nm、脉冲持续时间为 500 fs 的飞秒激光在钛板表面诱导 LIPSS 及 NPs 结构，这两种结构的峰谷高度差分别为(710±60) nm 和(250±80) nm。如图 17 所示，表面培养 48 h 后，LIPSS 结构和 NPs 结构表面的 *S. aureus* 附着相对于原始平坦表面明显减少。

Shaikh 等[163]使用蓝宝石脉冲激光器发射的波长为 800 nm、重复频率为 3 kHz、脉宽为 45 fs、能量密度为 0.6 J/cm^2 的飞秒激光照射样品表面，在 25 μm/s 和 800 μm/s 的扫描速度下于 Ti6Al4V 表面制备出了 Ti-1 和 Ti-2 两种微结构，然后用这两种结构体外培养 *S. aureus*、变形链球菌(*S. mutans*)和铜绿假单胞菌(*P. aeruginosa*)。结果显示：Ti-1 结构表面无 *S. aureus* 及 *S. mutans* 附着，存在零星 *P. aeruginosa* 菌落；Ti-2 表面显著抑制了 *S. mutans* 和 *P. aeruginosa* 的生长，但允许 *S. aureus* 菌落生长。Fadeeva 等[164]利用飞秒激光制备了如图 18 所示的两层微纳准周期自组织结构，用于模拟莲叶表面。*S. aureus* 及 *P. aeruginosa* 培养 18 h 后发现，微纳结构表面可以抑制 *P. aeruginosa* 生长而不能抑制 *S. aureus* 生长。Fadeeva 等分析后认为这与 *S. aureus* 为球状而 *P. aeruginosa* 为杆状有关。

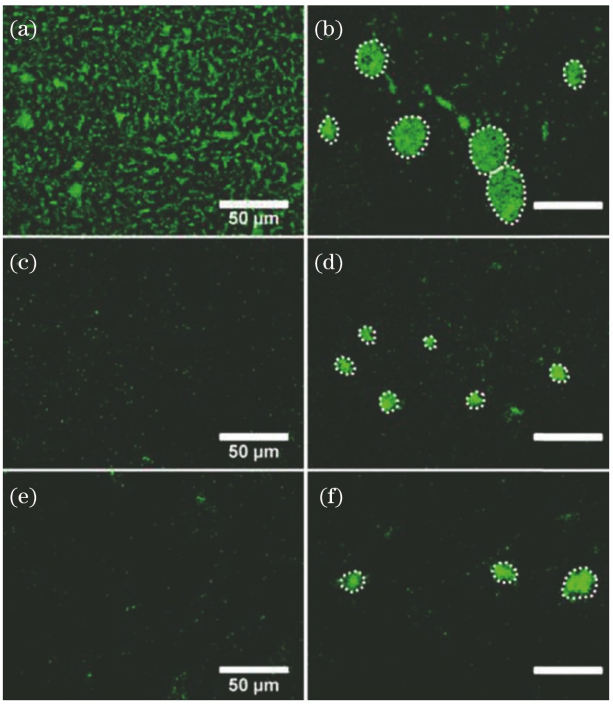

图 17 培养 48 h 后，钛板表面的 *S. aureus* 附着情况[162]。(a)～(b)原始表面；(c)～(d)LIPSS 表面；(e)～(f)NPs 表面

Fig. 17 Adhesion of *S. aureus* on titanium plate after 48 h culture[162]. (a)-(b) Original surface; (c)-(d) LIPSS surface; (e)-(f) NPs surface

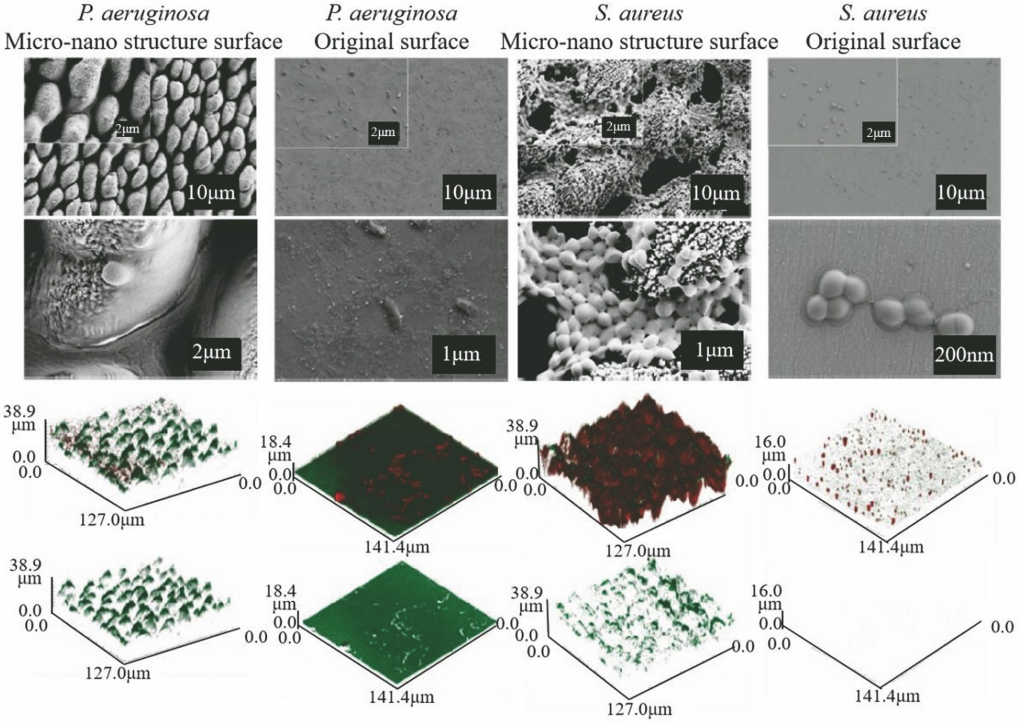

图 18 将 *P. aeruginosa* 及 *S. aureus* 在微纳结构及原始表面培养 18 h 后的 SEM 图像及激光扫描共聚焦显微镜(CLSM)图像，活细菌染为红色，胞外聚合物(EPS)染为绿色[164]

Fig. 18 SEM and CLSM images of *P. aeruginosa* and *S. aureus* cultured on micro/nano structure and original surfaces for 18 h, where live bacteria were stained red and EPS was stained green[164]

5 结束语

飞秒激光制备的钛合金及镁合金医用金属材料表面功能微结构在体液光谱检测、调控植入物表面细胞行为、口腔临床表面抗菌等方面具有良好表现：1)钛合金表面微结构可用于葡萄糖检测及蛋白体外光谱监测，可通过 SERS、SEF 或 SERS-SEF 双增强实现检测，其谱峰强度与待检测离子浓度具有良好的线性关系，检测限及灵敏度表现较好；2)镁合金表面微结构调控临床植入物表面细胞行为的研究结果显示，LIPSS 结构有利于细胞黏附，并可调控细胞按照特定方向迁移，刺激细胞增殖与分化；3)钛合金表面飞秒激光诱导微结构对口腔临床常见细菌，如牙龈卟啉单胞菌、大肠杆菌和金黄色葡萄球菌等，可以实现 90%及以上的抑制效果[165]（针对特定菌群，可以通过调控微结构实现选择性抑制）。

目前，飞秒激光诱导医用金属材料表面功能微纳结构仍需在以下几方面重点突破。

1）飞秒激光诱导微纳结构的调控机理

飞秒激光可以突破衍射极限对精度的限制，实现三维结构加工；然而，在超快时间尺度及极高能量等条件下，完善、清晰的飞秒激光-生物金属材料相互作用机理还有待进一步明晰与验证。目前关于飞秒激光诱导材料蚀除机理的研究主要存在有限区域等限制，缺乏多尺度、多模型耦合分析与实验验证。

2）功能微纳结构的前期设计

飞秒激光诱导沟槽结构、微孔结构引导细胞迁移分化机理等方面的研究报道近年来较为常见，而复合微纳结构对细菌/细胞行为影响的内在规律尚未真正明确。功能微纳结构设计有望进一步与生物力学、临床医学等多学科交叉，从而更加有效地指导加工制备和临床应用。

3）飞秒激光微纳加工工艺优化

飞秒激光加工技术的进步在很大程度上依赖光源进步，高能量、高重复频率光束是飞秒激光加工技术进步的动力。然而，光束能量提高会延长等离子体寿命，重复频率提升会增大等离子体与飞秒激光束相互作用的概率，从而对光束质量、形态产生影响，并且等离子体热效应会降低飞秒激光的加工精度。飞秒激光加工精度目前能够达到纳米级，加工效率主要依赖于并行模式，加工幅面扩大需要高端控制模块，工艺过程有待进一步优化提升。此外，加工过程多感官在线监测和实时调控成为下一步智能化加工研究的重点。

4）飞秒激光诱导功能微纳结构的临床实践

目前，飞秒激光诱导微纳结构功能的模拟验证环境较为单一，主要是针对单一细胞/细菌行为的验证。多细胞/细菌之间信号传递以及相互影响、长时间尺度上细胞/细菌行为的监测与调控等工作还有待进一步深入研究。飞秒激光诱导微纳结构植入体内后的临床表现将被作为后续研究中的重要衡量指标。针对植入物的复杂拓扑形状，实现飞秒激光诱导功能结构的大规模商业化制造与标准化检验仍有待进一步推进。

参 考 文 献

[1] Kurtz S, Mowat F, Ong K, et al. Prevalence of primary and revision total hip and knee arthroplasty in the United States from 1990 through 2002[J]. The Journal of Bone and Joint Surgery, 2005, 87(7): 1487-1497.

[2] 郑玉峰, 吴远浩. 处在变革中的医用金属材料[J]. 金属学报, 2017, 53(3): 257-297.
Zheng Y F, Wu Y H. Revolutionizing metallic biomaterials[J]. Acta Metallurgica Sinica, 2017, 53(3): 257-297.

[3] Breine U, Branemark P I, Johanson B. Regeneration of bone marrow. A clinical and experimental study (preliminary report)[J]. Acta Chirurgica Scandinavica, 1961, 122: 125-130.

[4] 张文毓. 生物医用金属材料研究现状与应用进展[J]. 金属世界, 2020(1): 21-27.
Zhang W Y. Research status and application progress of biomedical metal materials[J]. Metal World, 2020(1): 21-27.

[5] Deligianni D, Katsala N, Ladas S, et al. Effect of surface roughness of the titanium alloy Ti-6Al-4V on human bone marrow cell response and on protein adsorption[J]. Biomaterials, 2001, 22(11): 1241-1251.

[6] Scarano A, Piattelli M, Caputi S, et al. Bacterial adhesion on commercially pure titanium and zirconium oxide disks: an *in vivo* human study[J]. Journal of Periodontology, 2004, 75(2): 292-296.

[7] Niinomi M, Nakai M, Hieda J. Development of new metallic alloys for biomedical applications[J]. Acta Biomaterialia, 2012, 8(11): 3888-3903.

[8] Qu W T, Sun X G, Yuan B F, et al. Tribological behaviour of biomedical Ti-Zr-based shape memory alloys[J]. Rare Metals, 2017, 36(6): 478-484.

[9] Jin M, Lu X, Qiao Y, et al. Fabrication and characterization of anodic oxide nanotubes on TiNb

alloys[J]. Rare Metals, 2016, 35(2): 140-148.

[10] Oliveira N T C, Ferreira E A, Duarte L T, et al. Corrosion resistance of anodic oxides on the Ti-50Zr and Ti-13Nb-13Zr alloys[J]. Electrochimica Acta, 2006, 51(10): 2068-2075.

[11] Elias L M, Schneider S G, Schneider S, et al. Microstructural and mechanical characterization of biomedical Ti-Nb-Zr (-Ta) alloys[J]. Materials Science and Engineering A, 2006, 432(1/2): 108-112.

[12] Fukuda A, Takemoto M, Saito T, et al. Bone bonding bioactivity of Ti metal and Ti-Zr-Nb-Ta alloys with Ca ions incorporated on their surfaces by simple chemical and heat treatments[J]. Acta Biomaterialia, 2011, 7(3): 1379-1386.

[13] Ozan S, Lin J X, Li Y C, et al. New Ti-Ta-Zr-Nb alloys with ultrahigh strength for potential orthopedic implant applications[J]. Journal of the Mechanical Behavior of Biomedical Materials, 2017, 75: 119-127.

[14] Shadanbaz S, Dias G J. Calcium phosphate coatings on magnesium alloys for biomedical applications: a review[J]. Acta Biomaterialia, 2012, 8(1): 20-30.

[15] 郑玉峰, 夏丹丹, 谌雨农, 等. 增材制造可降解金属医用植入物[J]. 金属学报, 2021, 57(11): 1499-1520.
Zheng Y F, Xia D D, Chen Y N, et al. Additively manufactured biodegradable metal implants[J]. Acta Metallurgica Sinica, 2021, 57(11): 1499-1520.

[16] 陈军修, 王晓婉, 刘辰, 等. 生物可降解镁合金研究进展[J]. 特种铸造及有色合金, 2021, 41(10): 1273-1282.
Chen J X, Wang X W, Liu C, et al. Recent progress in the biodegradable magnesium alloys[J]. Special Casting & Nonferrous Alloys, 2021, 41(10): 1273-1282.

[17] Payr E. Beiträge zur technik der blutgefäss- und nervennaht nebst mittheilungen über die verwendung eines resorbirbaren metalles in der chirurgie[J]. Arch Klin Chir, 1990, 62: 67-93.

[18] Lambotte A. Technique et indications de la prothèse perdue dans le traitement des fractures[J]. Presse Medicale, 1909, 17: 321-323

[19] 郑玉峰, 刘彬, 顾雪楠. 可生物降解性医用金属材料的研究进展[J]. 材料导报, 2009, 23(1): 1-6.
Zheng Y F, Liu B, Gu X N. Research progress in biodegradable metallic materials for medical application[J]. Materials Review, 2009, 23(1): 1-6.

[20] 周宏博, 喻正文,刘建国. 医用金属植入材料促进骨再生的分子机制[J]. 中国组织工程研究, 2022, 26(10): 1588-1596.
Zhou H B, Yu Z W, Liu J G. Molecular mechanism of bone regeneration promoted by medical metal implant materials[J]. Chinese Journal of Tissue Engineering Research, 2022, 26(10): 1588-1596.

[21] Sheng J, Sheng X Y, La P Q, et al. *In-situ* tensile study of annealed bimodal nano/micro grained medical 316L stainless steel[J]. Ferroelectrics, 2019, 546(1): 158-168.

[22] 范燕, 徐昕荣, 石志峰, 等. 生物医用金属材料表面改性的研究进展[J]. 材料导报, 2020, 34(S2): 1327-1329.
Fan Y, Xu X R, Shi Z F, et al. Research progress of surface modification of biomedical metallic materials[J]. Materials Reports, 2020, 34(S2): 1327-1329.

[23] Xue X D, Ma C P, An H J, et al. Corrosion resistance and cytocompatibility of Ti-20Zr-10Nb-4Ta alloy surface modified by a focused fiber laser[J]. Science China Materials, 2018, 61(4): 516-524.

[24] Zarka M, Dikici B, Niinomi M, et al. The $Ti_{3.6}Nb_{1.0}Ta_{0.2}Zr_{0.2}$ coating on anodized aluminum by PVD: a potential candidate for short-time biomedical applications[J]. Vacuum, 2021, 192: 110450.

[25] Chopra D, Gulati K, Ivanovski S. Micro + nano: conserving the gold standard microroughness to nanoengineer zirconium dental implants[J]. ACS Biomaterials Science & Engineering, 2021, 7(7): 3069-3074.

[26] Chow D H K, Wang J L, Wan P, et al. Biodegradable magnesium pins enhanced the healing of transverse patellar fracture in rabbits[J]. Bioactive Materials, 2021, 6(11): 4176-4185.

[27] Qu X H, Yang H T, Jia B, et al. Zinc alloy-based bone internal fixation screw with antibacterial and anti-osteolytic properties[J]. Bioactive Materials, 2021, 6(12): 4607-4624.

[28] Gao Y, Huang W C, Yang C Y, et al. Targeted photothermal therapy of mice and rabbits realized by macrophage-loaded tungsten carbide[J]. Biomaterials Science, 2019, 7(12): 5350-5358.

[29] Sun Z H, Zhang X X, Xu D, et al. Silver-amplified fluorescence immunoassay via aggregation-induced emission for detection of disease biomarker[J]. Talanta, 2021, 225: 121963.

[30] 焦二龙, 孙宇, 肖睿, 等. 高熵合金 AlCoCrCuFeTi$_x$ 小鼠急性全身毒性及兔皮下植入实验研究[J]. 哈尔滨医科大学学报, 2019, 53(6): 571-575.
Jiao E L, Sun Y, Xiao R, et al. Study on the acute

systemic toxicity of high-entropy alloy AlCoCrCuFeTi$_x$ in mice and subcutaneous implantation in rabbits [J]. Journal of Harbin Medical University, 2019, 53(6): 571-575.

[31] Andrade C X, Quirynen M, Rosenberg D R, et al. Interaction between different implant surfaces and liquid fibrinogen: a pilot *in vitro* experiment [J]. BioMed Research International, 2021, 2021: 9996071.

[32] Wang Y Y, Gong P, Zhang J. Effects of different implant surface properties on the biological behavior of Schwann cells [J]. West China journal of stomatology, 2021, 39(3): 279-285.

[33] Ständert V, Borcherding K, Bormann N, et al. Antibiotic-loaded amphora-shaped pores on a titanium implant surface enhance osteointegration and prevent infections [J]. Bioactive Materials, 2021, 6(8): 2331-2345.

[34] Doloff J C, Veiseh O, de Mezerville R, et al. The surface topography of silicone breast implants mediates the foreign body response in mice, rabbits and humans [J]. Nature Biomedical Engineering, 2021, 5(10): 1115-1130.

[35] Li Y X, Li C, Yu R, et al. Application of polydopamine on the implant surface modification [J]. Polymer Bulletin, 2021: 1-21.

[36] Rieber H, Frontzek A, Heinrich S, et al. Microbiological diagnosis of polymicrobial periprosthetic joint infection revealed superiority of investigated tissue samples compared to sonicate fluid generated from the implant surface [J]. International Journal of Infectious Diseases, 2021, 106: 302-307.

[37] Barrère F, Mahmood T A, de Groot K, et al. Advanced biomaterials for skeletal tissue regeneration: instructive and smart functions [J]. Materials Science and Engineering R, 2008, 59(1/2/3/4/5/6): 38-71.

[38] Zaffora A, di Franco F, Virtù D, et al. Tuning of the Mg alloy AZ31 anodizing process for biodegradable implants[J]. ACS Applied Materials & Interfaces, 2021, 13(11): 12866-12876.

[39] Dong H Z, Virtanen S. Anodic ZnO microsheet coating on Zn with sub-surface microtrenched Zn layer reduces risk of localized corrosion and improves bioactivity of pure Zn[J]. Coatings, 2021, 11(5): 486.

[40] Aliasghari S, Skeldon P, Thompson G E. Plasma electrolytic oxidation of titanium in a phosphate/silicate electrolyte and tribological performance of the coatings [J]. Applied Surface Science, 2014, 316: 463-476.

[41] Çelik İ, Alsaran A, Purcek G. Effect of different surface oxidation treatments on structural, mechanical and tribological properties of ultrafine-grained titanium[J]. Surface and Coatings Technology, 2014, 258: 842-848.

[42] Heimann R B. Thermal spraying of biomaterials [J]. Surface and Coatings Technology, 2006, 201(5): 2012-2019.

[43] Lima R S, Marple B R. Thermal spray coatings engineered from nanostructured ceramic agglomerated powders for structural, thermal barrier and biomedical applications: a review [J]. Journal of Thermal Spray Technology, 2007, 16(1): 40-63.

[44] Lin Z, Li S J, Sun F, et al. Surface characteristics of a dental implant modified by low energy oxygen ion implantation[J]. Surface and Coatings Technology, 2019, 365: 208-213.

[45] Feng H Y, Yu Z L, Chu P K. Ion implantation of organisms[J]. Materials Science and Engineering R, 2006, 54(3/4): 49-120.

[46] Zhang Z Q, Zhang Y, Liu Y, et al. Electrodeposition of Nd^{3+}-doped metal-organic frameworks on titanium dioxide nanotube array coated by hydroxyapatite for anti-microbial and anticorrosive implant[J]. Ionics, 2021, 27(6): 2707-2715.

[47] Kumar R, Thanigaivelan R, Rajanikant G K, et al. Evaluation of hydroxyapatite- and zinc-coated Ti-6Al-4V surface for biomedical application using electrochemical process[J]. Journal of the Australian Ceramic Society, 2021, 57(1): 107-116.

[48] Liu W C, Wang H Y, Chen L C, et al. Hydroxyapatite/tricalcium silicate composites cement derived from novel two-step sol-gel process with good biocompatibility and applications as bone cement and potential coating materials[J]. Ceramics International, 2019, 45(5): 5668-5679.

[49] Owens G J, Singh R K, Foroutan F, et al. Sol-gel based materials for biomedical applications [J]. Progress in Materials Science, 2016, 77: 1-79.

[50] Sharma V, Prakash U, Kumar B V M. Surface composites by friction stir processing: a review[J]. Journal of Materials Processing Technology, 2015, 224: 117-134.

[51] Misra R D K, Thein-Han W W, Pesacreta T C, et al. Cellular response of preosteoblasts to nanograined/ultrafine-grained structures [J]. Acta Biomaterialia, 2009, 5(5): 1455-1467.

[52] Weng F, Chen C Z, Yu H J. Research status of

laser cladding on titanium and its alloys: a review [J]. Materials & Design, 2014, 58: 412-425.

[53] Kurella A, Dahotre N B. Review paper: surface modification for bioimplants: the role of laser surface engineering [J]. Journal of Biomaterials Applications, 2005, 20(1): 5-50.

[54] 潘瑞, 张红军, 钟敏霖. 三级微纳超疏水表面的超快激光复合制备及防除冰性能研究[J]. 中国激光, 2021, 48(2): 0202009.
Pan R, Zhang H J, Zhong M L. Ultrafast laser hybrid fabrication and ice-resistance performance of a triple-scale micro/nano superhydrophobic surface [J]. Chinese Journal of Lasers, 2021, 48(2): 0202009.

[55] du Plooy R, Akinlabi E T. Analysis of laser cladding of titanium alloy [J]. Materials Today: Proceedings, 2018, 5(9): 19594-19603.

[56] Long J Y, Fan P X, Gong D W, et al. Superhydrophobic surfaces fabricated by femtosecond laser with tunable water adhesion: from lotus leaf to rose petal [J]. ACS Applied Materials & Interfaces, 2015, 7(18): 9858-9865.

[57] Tian Y S, Chen C Z, Li S T, et al. Research progress on laser surface modification of titanium alloys[J]. Applied Surface Science, 2005, 242(1/2): 177-184.

[58] Um S H, Lee J, Song I S, et al. Regulation of cell locomotion by nanosecond-laser-induced hydroxyapatite patterning[J]. Bioactive Materials, 2021, 6(10): 3608-3619.

[59] Lee B E J, Exir H, Weck A, et al. Characterization and evaluation of femtosecond laser-induced sub-micron periodic structures generated on titanium to improve osseointegration of implants [J]. Applied Surface Science, 2018, 441: 1034-1042.

[60] Hsiao W T, Chang H C, Nanci A, et al. Surface microtexturing of Ti-6Al-4V using an ultraviolet laser system [J]. Materials & Design, 2016, 90: 891-895.

[61] Kumari R, Scharnweber T, Pfleging W, et al. Laser surface textured titanium alloy (Ti-6Al-4V)-part II: studies on bio-compatibility [J]. Applied Surface Science, 2015, 357: 750-758.

[62] 阿占文, 吴影, 肖宇, 等. 超快激光微孔加工工艺研究进展[J]. 中国激光, 2021, 48(8): 0802013.
A Z W, Wu Y, Xiao Y, et al. Research progresses of process technology in ultrafast laser micro-hole drilling[J]. Chinese Journal of Lasers, 2021, 48(8): 0802013.

[63] 史雪松, 姜澜, 李欣. 电子动态调控的飞秒激光表面微纳结构可控制造新方法及其应用[J]. 机械工程学报, 2018, 54(4): 56.
Shi X S, Jiang L, Li X. New method and application of electronically dynamically controlled femtosecond laser surface micro nano structure controllable manufacturing[J]. Journal of Mechanical Engineering, 2018, 54(4): 56.

[64] Liu W, Liu S F, Wang L Q. Surface modification of biomedical titanium alloy: micromorphology, microstructure evolution and biomedical applications [J]. Coatings, 2019, 9(4): 249.

[65] Kumar K K, Samuel G L, Shunmugam M S. Theoretical and experimental investigations of ultra-short pulse laser interaction on Ti6Al4V alloy[J]. Journal of Materials Processing Technology, 2019, 263: 266-275.

[66] 姜澜, 胡洁, 王国燕, 等. 电子动态调控超快激光微纳制造[J]. 中国基础科学, 2016, 18(5): 11-27.
Jiang L, Hu J, Wang G Y, et al. Ultrafast laser micro/nano fabrication based on electrons dynamics control[J]. China Basic Science, 2016, 18(5): 11-27.

[67] 陈念科, 黄宇婷, 李贤斌, 等. 超快激光诱导固体非热相变及其原子机理进展[J]. 中国激光, 2021, 48(2): 0202001.
Chen N K, Huang Y T, Li X B, et al. Recent progress on ultrafast laser-induced solid nonthermal phase transitions and atomic mechanisms [J]. Chinese Journal of Lasers, 2021, 48(2): 0202001.

[68] Lewis L J, Perez D. Laser ablation with short and ultrashort laser pulses: basic mechanisms from molecular-dynamics simulations[J]. Applied Surface Science, 2009, 255(10): 5101-5106.

[69] 白雪, 陈烽. 飞秒激光制备超疏水表面的研究进展[J]. 光学学报, 2021, 41(1): 0114003.
Bai X, Chen F. Recent advances in femtosecond laser-induced superhydrophobic surfaces [J]. Acta Optica Sinica, 2021, 41(1): 0114003.

[70] Li X X, Guan Y C. Theoretical fundamentals of short pulse laser-metal interaction: a review [J]. Nanotechnology and Precision Engineering, 2020, 3: 105-125.

[71] Bruneau S, Hermann J, Dumitru G, et al. Ultra-fast laser ablation applied to deep-drilling of metals [J]. Applied Surface Science, 2005, 248(1/2/3/4): 299-303.

[72] 苏高世. 基于电子动态调控的超快激光微纳加工多尺度理论研究[D]. 北京: 北京理工大学, 2018: 12-20.
Su G S. Multiscale theoretical research on ultrafast laser micro nano machining based on electronic dynamic regulation[D]. Beijing: Beijing Institute of

Technology, 2018: 12-20.

[73] Li S C, Li S Y, Zhang F J, et al. Possible evidence of Coulomb explosion in the femtosecond laser ablation of metal at low laser fluence[J]. Applied Surface Science, 2015, 355: 681-685.

[74] 吴雪峰, 梅三林. 飞秒激光加工机理及仿真研究进展[J]. 激光与光电子学进展, 2021, 58(19): 1900005.
Wu X F, Mei S L. Research progress in femtosecond laser machining mechanism and simulation analysis[J]. Laser & Optoelectronics Progress, 2021, 58(19): 1900005.

[75] Shugaev M V, Wu C P, Armbruster O, et al. Fundamentals of ultrafast laser-material interaction [J]. MRS Bulletin, 2016, 41(12): 960-968.

[76] Wu C P, Zhigilei L V. Microscopic mechanisms of laser spallation and ablation of metal targets from large-scale molecular dynamics simulations[J]. Applied Physics A, 2014, 114(1): 11-32.

[77] 王春艳, 顾寅, 施锣佳, 等. 体液检测技术的发展及在航天医学研究中应用展望[J]. 生命科学仪器, 2019, 17(6): 3-19.
Wang C Y, Gu Y, Shi L J, et al. Development of humoral detection technology and its application prospect in space medicine research[J]. Life Science Instruments, 2019, 17(6): 3-19.

[78] 吕静. 导致体液标本检验不合格的原因及预防措施[J]. 中国医药指南, 2021, 19(8): 103-104.
Lü J. Causes and preventive measures of unqualified body fluid samples[J]. Guide of China Medicine, 2021, 19(8): 103-104.

[79] Xiao G D, Dong D M, Liao T Q, et al. Detection of pesticide (chlorpyrifos) residues on fruit peels through spectra of volatiles by FTIR[J]. Food Analytical Methods, 2015, 8(5): 1341-1346.

[80] Guo P Z, Sikdar D, Huang X Q, et al. Plasmonic core-shell nanoparticles for SERS detection of the pesticide thiram: size- and shape-dependent Raman enhancement[J]. Nanoscale, 2015, 7(7): 2862-2868.

[81] 邱梦情, 徐青山, 郑守国, 等. 农药残留检测中表面增强拉曼光谱的研究进展[J]. 光谱学与光谱分析, 2021, 41(11): 3339-3346.
Qiu M Q, Xu Q S, Zheng S G, et al. Research progress of surface-enhanced Raman spectroscopy in pesticide residue detection[J]. Spectroscopy and Spectral Analysis, 2021, 41(11): 3339-3346.

[82] 周赛, 陈瑞, 段美, 等. 表面增强拉曼散射技术在生物医学领域的研究进展[J]. 化工技术与开发, 2020, 49(S1): 57-61.
Zhou S, Chen R, Duan M, et al. Research progress of surface enhanced Raman scattering in biomedical field[J]. Technology & Development of Chemical Industry, 2020, 49(S1): 57-61.

[83] Fleischmann M, Hendra P J, McQuillan A J. Raman spectra of pyridine adsorbed at a silver electrode[J]. Chemical Physics Letters, 1974, 26(2): 163-166.

[84] Zhou W, Zeng J W, Li X F, et al. Ultraviolet Raman spectra of double-resonant modes of graphene[J]. Carbon, 2016, 101: 235-238.

[85] Tschirner N, Lange H, Schliwa A, et al. Interfacial alloying in CdSe/CdS heteronanocrystals: a Raman spectroscopy analysis[J]. Chemistry of Materials, 2012, 24(2): 311-318.

[86] Li H, Sun Z Y, Zhong W Y, et al. Ultrasensitive electrochemical detection for DNA arrays based on silver nanoparticle aggregates[J]. Analytical Chemistry, 2010, 82(13): 5477-5483.

[87] 邹婷婷, 徐振林, 杨金易, 等. 表面增强拉曼光谱技术在食品安全检测中的应用研究进展[J]. 分析测试学报, 2018, 37(10): 1174-1181.
Zou T T, Xu Z L, Yang J Y, et al. Application advances of surface enhanced Raman spectroscopy in food safety detection[J]. Journal of Instrumental Analysis, 2018, 37(10): 1174-1181.

[88] 封昭, 周骏, 陈栋, 等. 基于金/银纳米三明治结构SERS特性的超灵敏前列腺特异性抗原检测[J]. 发光学报, 2015, 36(9): 1064-1070.
Feng Z, Zhou J, Chen D, et al. Hypersensitization immunoassay of prostate-specific antigen based on SERS of sandwich-type Au/Ag nanostructure[J]. Chinese Journal of Luminescence, 2015, 36(9): 1064-1070.

[89] Sun Q Y, Zhang Y Q, Sun L X, et al. Microscopic surface plasmon enhanced Raman spectral imaging [J]. Optics Communications, 2017, 392: 64-67.

[90] Qian X M, Nie S M. Single-molecule and single-nanoparticle SERS: from fundamental mechanisms to biomedical applications[J]. Chemical Society Reviews, 2008, 37(5): 912-920.

[91] Ding S Y, Yi J, Li J F, et al. Nanostructure-based plasmon-enhanced Raman spectroscopy for surface analysis of materials[J]. Nature Reviews Materials, 2016, 1: 16021.

[92] Schatz G, Young M A, Duyne R P. Electromagnetic mechanism of SERS[M]// Katrin K, Martin M, Harald K. Surface-enhanced Raman scattering. Germany: Springer-Verlag, 2006, 103: 19-45.

[93] Moskovits M. Surface-enhanced spectroscopy[J]. Reviews of Modern Physics, 1985, 57(3): 783-826.

[94] Otto A. Surface enhanced Raman scattering[J]. Vacuum, 1983, 33(10/11/12): 797-802.

[95] Ueba H. Theory of charge transfer excitation in surface enhanced Raman scattering[J]. Surface Science, 1983, 131(2/3): 347-366.

[96] Sharma B, Bugga P, Madison L R, et al. Bisboronic acids for selective, physiologically relevant direct glucose sensing with surface-enhanced Raman spectroscopy[J]. Journal of the American Chemical Society, 2016, 138(42): 13952-13959.

[97] Cai J, Huang J, Ge M, et al. Immobilization of Pt nanoparticles via rapid and reusable electropolymerization of dopamine on TiO_2 nanotube arrays for reversible SERS substrates and nonenzymatic glucose sensors[J]. Small, 2017, 13(19): 1604240.

[98] Dinish U S, Yaw F C, Agarwal A, et al. Development of highly reproducible nanogap SERS substrates: comparative performance analysis and its application for glucose sensing[J]. Biosensors and Bioelectronics, 2011, 26(5): 1987-1992.

[99] Sooraj K P, Ranjan M, Rao R, et al. SERS based detection of glucose with lower concentration than blood glucose level using plasmonic nanoparticle arrays[J]. Applied Surface Science, 2018, 447: 576-581.

[100] Xu L M, Liu H G, Zhou H, et al. One-step fabrication of metal nanoparticles on polymer film by femtosecond LIPAA method for SERS detection[J]. Talanta, 2021, 228: 122204.

[101] Luo X, Liu W J, Chen C H, et al. Femtosecond laser micro-nano structured Ag SERS substrates with unique sensitivity, uniformity and stability for food safety evaluation[J]. Optics & Laser Technology, 2021, 139: 106969.

[102] Huang Z, He W T, Shen H, et al. $NiCo_2S_4$ microflowers as peroxidase mimic: a multi-functional platform for colorimetric detection of glucose and evaluation of antioxidant behavior[J]. Talanta, 2021, 230: 122337.

[103] Zhao Z T, Li Q G, Sun Y J, et al. Highly sensitive and portable electrochemical detection system based on AuNPs @ CuO NWs/Cu_2O/CF hierarchical nanostructures for enzymeless glucose sensing[J]. Sensors and Actuators B, 2021, 345: 130379.

[104] Zhang Y, Li Y, Jia X, et al. Advanced electrochromic/electrofluorochromic poly(amic acid) toward the colorimetric/fluorometric dual-determination of glycosuria[J]. Materials Today Chemistry, 2021, 21: 100497.

[105] Ramos-Soriano J, Benitez-Benitez S J, Davis A P, et al. Inside cover: a vibration-induced-emission-based fluorescent chemosensor for the selective and visual recognition of glucose[J]. Angewandte Chemie International Edition, 2021, 60(31): 16718.

[106] Cui Z Q, Lu L B, Guan Y C, et al. Enhancing SERS detection on a biocompatible metallic substrate for diabetes diagnosing[J]. Optics Letters, 2021, 46(15): 3801-3804.

[107] 徐良敏, 张正龙, 蔡晓燕, 等. 金属表面荧光增强的物理增强机制[J]. 发光学报, 2009, 30(3): 373-378.
Xu L M, Zhang Z L, Cai X Y, et al. Physical mechanisms of fluorescence enhancement at metal surface[J]. Chinese Journal of Luminescence, 2009, 30(3): 373-378.

[108] 赵星, 董军, 高伟, 等. 表面增强荧光效应研究进展[J]. 激光技术, 2018, 42(4): 511-520.
Zhao X, Dong J, Gao W, et al. Progresses of surface enhanced fluorescence[J]. Laser Technology, 2018, 42(4): 511-520.

[109] Zhong B B, Zu X H, Yi G B, et al. Fluorescence enhancement of the conjugated polymer films based on well-ordered Au nanoparticle arrays[J]. Journal of Nanoparticle Research, 2016, 18(9): 281.

[110] Yin Y Q, Sun Y, Yu M, et al. ZnO nanorod array grown on Ag layer: a highly efficient fluorescence enhancement platform[J]. Scientific Reports, 2015, 5: 8152.

[111] Viktor I S, Hacı A, Aleksandr A K, et al. Simulation of the effect of argon pressure on thermal processes in the sputtering unit of a magnetron with a hot target[J]. Vacuum, 2021, 192: 110421.

[112] Ding L, Zhao Y Y, Li H H, et al. A highly selective ratiometric fluorescent probe for doxycycline based on the sensitization effect of bovine serum albumin[J]. Journal of Hazardous Materials, 2021, 416: 125759.

[113] Zhang J R, Hu G Q, Lu L B, et al. Enhancing protein fluorescence detection through hierarchical biometallic surface structuring[J]. Optics Letters, 2019, 44(2): 339-342.

[114] Kamalieva A N, Toropov N A, Bogdanov K V, et al. Enhancement of fluorescence and Raman scattering in cyanine-dye molecules on the surface of silicon-coated silver nanoparticles[J]. Optics and Spectroscopy, 2018, 124(3): 319-322.

[115] Cao Q, Wang X Y, Cui Q L, et al. Synthesis and application of bifunctional gold/gelatin nanocomposites with enhanced fluorescence and

Raman scattering[J]. Colloids and Surfaces A, 2017, 514: 117-125.

[116] Cyrankiewicz M, Wybranowski T, Kruszewski S. Silver nanoparticles as enhancing substrates for Raman and fluorescence spectroscopy[J]. Acta Physica Polonica A, 2014, 125(4A): 11-15.

[117] Chang S, Eichmann S L, Huang T Y S, et al. Controlled design and fabrication of SERS-SEF multifunctional nanoparticles for nanoprobe applications: morphology-dependent SERS phenomena[J]. The Journal of Physical Chemistry C, 2017, 121(14): 8070-8076.

[118] Lu L B, Zhang J R, Jiao L S, et al. Large-scale fabrication of nanostructure on bio-metallic substrate for surface enhanced Raman and fluorescence scattering[J]. Nanomaterials, 2019, 9(7): 916.

[119] 蔡彦坤, 祁星颖, 隋磊. 种植材料表面纳米级形貌对细胞成骨效应的影响[J]. 实用口腔医学杂志, 2019, 35(6): 891-894.
Cai Y K, Qi X Y, Sui L. Effect of nano morphology of implant material surface on cell osteogenesis[J]. Journal of Practical Stomatology, 2019, 35(6): 891-894.

[120] Huang Q L, Elkhooly T A, Liu X J, et al. Effects of hierarchical micro/nano-topographies on the morphology, proliferation and differentiation of osteoblast-like cells[J]. Colloids and Surfaces B, 2016, 145: 37-45.

[121] Palin E, Liu H N, Webster T J. Mimicking the nanofeatures of bone increases bone-forming cell adhesion and proliferation[J]. Nanotechnology, 2005, 16(9): 1828-1835.

[122] Mukherjee S, Dhara S, Saha P. Enhancing the biocompatibility of Ti6Al4V implants by laser surface microtexturing: an *in vitro* study[J]. The International Journal of Advanced Manufacturing Technology, 2015, 76(1/2/3/4): 5-15.

[123] 沈嘉炜. 生物分子在纳米材料表面的吸附及纳米孔道中的输运行为[D]. 杭州: 浙江大学, 2009: 3-5.
Shen J W. Adsorption and transportation behaviors of biomolecules on nanomaterial surfaces and in nanopores[D]. Hangzhou: Zhejiang University, 2009: 3-5.

[124] Omanovic S, Roscoe S G. Electrochemical studies of the adsorption behavior of bovine serum albumin on stainless steel[J]. Langmuir, 1999, 15(23): 8315-8321.

[125] Kidoaki S, Matsuda T. Adhesion forces of the blood plasma proteins on self-assembled monolayer surfaces of alkanethiolates with different functional groups measured by an atomic force microscope[J]. Langmuir, 1999, 15(22): 7639-7646.

[126] Laggoun R, Ferhat M, Saidat B, et al. Effect of p-toluenesulfonyl hydrazide on copper corrosion in hydrochloric acid solution[J]. Corrosion Science, 2020, 165: 108363.

[127] 王鲁宁, 刘丽君, 岩雨, 等. 蛋白质吸附对医用金属材料体外腐蚀行为的影响[J]. 金属学报, 2021, 57(1): 1-15.
Wang L N, Liu L J, Yan Y, et al. Influences of protein adsorption on the *in vitro* corrosion of biomedical metals[J]. Acta Metallurgica Sinica, 2021, 57(1): 1-15.

[128] Strehmel C, Perez-Hernandez H, Zhang Z F, et al. Geometric control of cell alignment and spreading within the confinement of antiadhesive poly (ethylene glycol) microstructures on laser-patterned surfaces[J]. ACS Biomaterials Science & Engineering, 2015, 1(9): 747-752.

[129] Vignesh R, Sakthinathan G, Velusamy R, et al. An *in-vitro* evaluation study on the effects of surface modification via physical vapor deposition on the degradation rates of magnesium-based biomaterials [J]. Surface and Coatings Technology, 2021, 411: 126972.

[130] Yang K H, Ger M D, Hwu W H, et al. Study of vanadium-based chemical conversion coating on the corrosion resistance of magnesium alloy[J]. Materials Chemistry and Physics, 2007, 101(2/3): 480-485.

[131] Chen J X, Zhang Y, Ibrahim M, et al. *In vitro* degradation and antibacterial property of a copper-containing micro-arc oxidation coating on Mg-2Zn-1Gd-0.5Zr alloy[J]. Colloids and Surfaces B, 2019, 179: 77-86.

[132] Iaroslav G, Maksym P, Roman V, et al. Cell and tissue response to nanotextured Ti6Al4V and Zr implants using high-speed femtosecond laser-induced periodic surface structures[J]. Nanomedicine: Nanotechnology, Biology and Medicine, 2019, 21: 102036.

[133] Xue X D, Lu L B, He D L, et al. Antibacterial properties and cytocompatibility of Ti-20Zr-10Nb-4Ta alloy surface with Ag microparticles by laser treatment[J]. Surface & Coatings Technology, 2021, 425: 127716.

[134] Czyż K, Marczak J, Major R, et al. Selected laser methods for surface structuring of biocompatible diamond-like carbon layers[J]. Diamond and Related Materials, 2016, 67: 26-40.

[135] Kennedy O O, Yoshikiyo K, Taiji A. Controlling macroscale cell alignment in self-organized cell

sheets by tuning the microstructure of adhesion-limiting micromesh scaffolds[J]. Materials Today Advances, 2021, 12: 100194.

[136] Dumas V, Guignandon A, Vico L, et al. Femtosecond laser nano/micro patterning of titanium influences mesenchymal stem cell adhesion and commitment[J]. Biomedical Materials, 2015, 10(5): 055002.

[137] Zhang J R, Guan Y C, Lin W T, et al. Enhanced mechanical properties and biocompatibility of Mg-Gd-Ca alloy by laser surface processing[J]. Surface and Coatings Technology, 2019, 362: 176-184.

[138] Willbold E, Weizbauer A, Loos A, et al. Magnesium alloys: a stony pathway from intensive research to clinical reality. Different test methods and approval-related considerations[J]. Journal of Biomedical Materials Research A, 2017, 105(1): 329-347.

[139] 张佳茹, 管迎春. 超快激光制备生物医用材料表面功能微结构的现状及研究进展[J]. 中国光学, 2019, 12(2): 199-213.
Zhang J R, Guan Y C. Surface functional microstructure of biomedical materials prepared by ultrafast laser: a review[J]. Chinese Optics, 2019, 12(2): 199-213.

[140] Martínez-Calderon M, Manso-Silván M, Rodríguez A, et al. Surface micro- and nano-texturing of stainless steel by femtosecond laser for the control of cell migration[J]. Scientific Reports, 2016, 6: 36296.

[141] Nuutinen T, Silvennoinen M, Päivänsaari K, et al. Control of cultured human cells with femtosecond laser ablated patterns on steel and plastic surfaces [J]. Biomedical Microdevices, 2013, 15(2): 279-288.

[142] Zhang J R, Lin W T, Guan Y C, et al. Biocompatibility enhancement of Mg-Gd-Ca alloy by laser surface modification[J]. Journal of Laser Applications, 2019, 31(2): 022510.

[143] Xiang T, Hou J W, Xie, Hui, et al. Biomimetic micro/nano structures for biomedical applications [J]. Nano Today, 2020, 35: 100980.

[144] Takayama I, Kondo N, Kalies S, et al. Myoblast adhesion and proliferation on biodegradable polymer films with femtosecond laser-fabricated micro through-holes[J]. Journal of Biophotonics, 2020, 13(7): e202000037.

[145] Cunha A, Zouani O F, Plawinski L, et al. Human mesenchymal stem cell behavior on femtosecond laser-textured Ti-6Al-4V surfaces[J]. Nanomedicine, 2015, 10(5): 725-739.

[146] Ma C P, Peng G, Nie L, et al. Laser surface modification of Mg-Gd-Ca alloy for corrosion resistance and biocompatibility enhancement[J]. Applied Surface Science, 2018, 445: 211-216.

[147] 梁春永, 李宝发, 王洪水, 等. 镁合金表面飞秒激光制备促骨细胞生长显微结构[J]. 稀有金属材料与工程, 2014, 43(S1): 253-256.
Liang C Y, Li B F, Wang H S, et al. Femtosecond lasers induced micropatterns on magnesium alloy to promote cell proliferation[J]. Rare Metal Materials and Engineering, 2014, 43(S1): 253-256.

[148] Yang Y W, He C X, E D Y, et al. Mg bone implant: features, developments and perspectives [J]. Materials & Design, 2020, 185: 108259.

[149] Chauhan P S, Kumarasamy M, Carcaboso A M, et al. Multifunctional silica-coated mixed polymeric micelles for integrin-targeted therapy of pediatric patient-derived glioblastoma[J]. Materials Science and Engineering C, 2021, 128: 112261.

[150] Godoy-Gallardo M, Eckhard U, Delgado L M, et al. Antibacterial approaches in tissue engineering using metal ions and nanoparticles: from mechanisms to applications[J]. Bioactive Materials, 2021, 6(12): 4470-4490.

[151] Jenkins J, Mantell J, Neal C, et al. Antibacterial effects of nanopillar surfaces are mediated by cell impedance, penetration and induction of oxidative stress[J]. Nature Communications, 2020, 11: 1626.

[152] Tripathy A, Sen P, Su B, et al. Natural and bioinspired nanostructured bactericidal surfaces[J]. Advances in Colloid and Interface Science, 2017, 248: 85-104.

[153] Schlaich C, Wei Q, Haag R. Mussel-inspired polyglycerol coatings with controlled wettability: from superhydrophilic to superhydrophobic surface coatings[J]. Langmuir: the ACS Journal of Surfaces and Colloids, 2017, 33(38): 9508-9520.

[154] Pogodin S, Hasan J, Baulin V A, et al. Biophysical model of bacterial cell interactions with nanopatterned cicada wing surfaces[J]. Biophysical Journal, 2013, 104(4): 835-840.

[155] Li X L. Bactericidal mechanism of nanopatterned surfaces[J]. Physical Chemistry Chemical Physics: PCCP, 2016, 18(2): 1311-1316.

[156] Xue F D, Liu J J, Guo L F, et al. Theoretical study on the bactericidal nature of nanopatterned surfaces [J]. Journal of Theoretical Biology, 2015, 385: 1-7.

[157] Kelleher S M, Habimana O, Lawler J, et al. Cicada wing surface topography: an investigation into the bactericidal properties of nanostructural features[J].

ACS Applied Materials & Interfaces, 2016, 8(24): 14966-14974.

[158] 高党鸽, 赵洲洋, 吕斌, 等. 超疏水抗菌表面的研究进展[J]. 精细化工, 2021, 38(5): 874-881.
Gao D G, Zhao Z Y, Lü B, et al. Research process of superhydrophobic antibacterial surfaces[J]. Fine Chemicals, 2021, 38(5): 874-881.

[159] Li Q Q, Bao X G, Sun J E, et al. Fabrication of superhydrophobic composite coating of hydroxyapatite/stearic acid on magnesium alloy and its corrosion resistance, antibacterial adhesion[J]. Journal of Materials Science, 2021, 56(8): 5233-5249.

[160] Hizal F, Rungraeng N, Lee J, et al. Nanoengineered superhydrophobic surfaces of aluminum with extremely low bacterial adhesivity [J]. ACS Applied Materials & Interfaces, 2017, 9(13): 12118-12129.

[161] 王瑞, 周延民. 种植材料表面飞秒激光掺银改性的抗菌性[J]. 中国老年学杂志, 2013, 33(10): 2307-2309.
Wang R, Zhou Y M. Antibacterial properties of planting materials modified by femtosecond laser silver doping[J]. Chinese Journal of Gerontology, 2013, 33(10): 2307-2309.

[162] Cunha A, Elie A M, Plawinski L, et al. Femtosecond laser surface texturing of titanium as a method to reduce the adhesion of Staphylococcus aureus and biofilm formation[J]. Applied Surface Science, 2016, 360: 485-493.

[163] Shaikh S, Kedia S, Singh D, et al. Surface texturing of Ti6Al4V alloy using femtosecond laser for superior antibacterial performance[J]. Journal of Laser Applications, 2019, 31(2): 022011.

[164] Fadeeva E, Truong V K, Stiesch M, et al. Bacterial retention on superhydrophobic titanium surfaces fabricated by femtosecond laser ablation [J]. Langmuir, 2011, 27(6): 3012-3019.

[165] Wu H, Liu T, Xu Z Y, et al. Enhanced bacteriostatic activity, osteogenesis and osseointegration of silicon nitride/polyetherketoneketone composites with femtosecond laser induced micro/nano structural surface [J]. Applied Materials Today, 2020, 18: 100523.

Progress in Preparation of Medical Functional Surfaces by Femtosecond Laser-Induced Micro/Nanostructures

Wang Yimeng[1], Guan Yingchun[1,2,3,4*]

[1] *School of Mechanical Engineering and Automation, Beihang University, Beijing* 100083, *China*;

[2] *National Engineering Laboratory of Additive Manufacturing for Large Metallic Components, Beihang University, Beijing* 100083, *China*;

[3] *International Research Institute for Multidisciplinary Science, Beihang University, Beijing* 100083, *China*;

[4] *Ningbo Innovation Research Institute, Beihang University, Ningbo* 315800, *Zhejiang, China*

Abstract

Significance Due to population aging and change in the modern lifestyle, tens of thousands of people are troubled by orthopedic, oral, and facial diseases. The demand for high-quality medical devices and implants in clinical medicine is increasing. Compared with traditional inorganic nonmetallic and polymer materials, metal materials have better biomechanical properties and processing ability. The surface state of medical devices and implants is an important factor in therapeutic schedules since it affects the complex biological behavior of nearby tissues, such as cell proliferation and differentiation, bone integration, immune response, neurotransmitter release and transport, bacterial infection, and so on. To promote innovation and development in the medical field, it is imperative to develop a simple, efficient, practical, and reliable preparation method for high-performance biological functional surfaces of typical medical devices and clinical implants.

Recently, many methods for modifying surfaces of medical metal materials have been developed. Various research methods focus on regulating the corrosion resistance and degradation rate of implants, blocking the release of harmful elements, promoting the adaptation of mechanical properties between implants and biological tissues, increasing biocompatibility, and obtaining antibacterial surfaces. Common surface modification methods include anodic oxidation, micro-arc oxidation, plasma spraying, ion implantation, electrochemical deposition, sol-gel,

friction stir treatment, etc.

Laser surface modification controls the accuracy characteristics of the implanted surface with high efficiency, no pollution, and low material consumption. It is widely applied to preparing periodic micro/nanostructures on the surface of several materials, providing a new idea for the surface modification of metal materials. Unlike the thermal effect caused by molecular vibration induced by a long-wavelength laser, the femtosecond laser has a very low pulse width. Low pulse energy can obtain high peak power, trigger multiphoton absorption and achieve material removal. The thermal effect in femtosecond laser processing can be ignored and the spatial selective manipulation of microstructure can be realized. Femtosecond lasers are suitable for quasi three-dimensional machining of all materials with high machining resolution. Femtosecond lasers are widely used in the preparation of biological functional surfaces.

Progress Body fluid detection provides an early specific indicator for assessing the health status. It requires stable detection method, high sensitivity, and reproducibility. Researchers have prepared femtosecond laser-induced periodic micro-nanostructures on the surface of titanium alloy. Surface-enhanced Raman scattering (SERS) and surface-enhanced fluorescence (SEF) detection substrates (Figs. 6 and 8) were used for glucose detection and *in vitro* spectral monitoring of protein. The spectral peak intensity has good linearity with the ion concentration to be detected, and the limit of detection (LOD) concentration and sensitivity is good. Thus, the SERS-SEF double enhancement substrate was prepared using the femtosecond laser for urine glucose detection (Fig. 9). The Raman and fluorescence enhancement factors were 7.85×10^{5} and 14.32, respectively, and the LOD was 14.4 mol/L. Additionally, titanium alloy detection substrate was prepared using femtosecond laser-induced surface periodic micro/nanostructure, providing a new idea for body fluid spectral selection and multitarget recognition and detection.

The surface morphology of materials is an important factor affecting the cell behavior on the surface of implants. It is directly related to the subsequent cell proliferation and osteogenic differentiation and is essential in the success or failure of the implant quality scheme. In the study of femtosecond laser-induced surface microstructure regulating the surface cell behavior of clinical implants, laser-induced periodic surface structure (LIPSS), nanopillars (NPs), microgroove, and micropore structure were studied more, among which LIPSS performs well. Femtosecond laser-induced LIPSS is conducive to cell adhesion and serves as a signal to regulate cell migration in a specific direction and stimulate cell proliferation and differentiation (Figs. 11 and 13). One-top femtosecond laser direct writing layered or composite periodic micro/nanostructure of degradable magnesium alloy realizes the increase of cell adhesion on the surface of degradable magnesium alloy, induces cell anisotropic migration and promotes osteoblast bone integration, which provides a new scheme for the clinical application of degradable magnesium alloy.

Presently, the mechanism of microstructure realizing antibacterial function is that the contact/suspension interaction between bacteria and microstructure leads to cell body rupture (Fig. 15) and surface superhydrophobic inhibition of bacterial biofilm formation (Fig. 16). The femtosecond laser induced micro/nanostructured on the surface of titanium alloy not only realized the inhibition of bacteria, such as *E. coli*, *S. aureus*, *P. gingivalis*, which are common in the oral clinic, but also obtained the selective inhibition of colonies (Fig. 18). Furthermore, its surface is nontoxic to cells, which provides an effective method to avoid implant infection and inflammation.

Conclusion and Prospect Presently, due to the lack of clear biomedical theoretical guidance in the early design of femtosecond laser surface micro/nanostructure technology, the functional effectiveness of micro/nanostructure depends on subsequent experimental verification. Additionally, the simulation and verification environment of the micro/nanostructure function surfaces is relatively single, such as for single-cell/bacterial behavior, signal transmission, and interaction between multiple cells/bacteria, monitoring and regulation of cell/bacterial behavior on a long time scale need to be further studied.

Key words laser technique; femtosecond laser; micro/nanostructure; function surface; biocompatibility; spectral detection